m^{6}A-mRNA reader *YTHDF2* identified as a potential risk gene in autism with disproportionate megalencephaly

Short running title: Megalencephaly autism risk genes

Sierra S. Nishizaki[1,2,3,4], Nicholas K. Haghani[1,5], Gabriana N. La[1,5], Natasha Ann F. Mariano[1,6], José M. Uribe-Salazar[1,5], Gulhan Kaya[1], Melissa Regester[3,4], Derek Sayre Andrews[3,4], Christine Wu Nordahl[3,4], David G. Amaral[3,4], Megan Y. Dennis[1,3,4,5†]

[1]Genome Center, [2]Autism Research Training Program, [3]Department of Psychiatry and Behavioral Sciences, [4]MIND Institute, [5]Department of Biochemistry & Molecular Medicine, [6]Postbaccalaureate Research Education Program, University of California Davis, CA, USA

[†]Corresponding author:
Megan Y. Dennis, Ph.D.
University of California, Davis
School of Medicine
One Shields Avenue
Genome Center, 4303 GBSF
Davis, CA 95616
Email: mydennis@ucdavis.edu

Acknowledgements: Thank you to the Autism Phenome Project (APP) research staff, especially Dr. Brianna Heath, and clinical recommendations from Dr. Suma Shankar, as well as the undergraduate students that provide husbandry and care for our zebrafish. We are grateful to Dr. Bruce Appel from the University of Colorado for sharing the HuC-eGFP line. A special thank you to the families who have generously shared their genetic data – you are who all of this research is for.

Data availability statement: Raw sequencing data of patients, including FASTQ and VCF files, can be accessed through the MSSNG access agreement (https://research.mss.ng) and the Simons Simplex Collection through SFARI Base (https://www.sfari.org/resource/sfari-base/). Transcriptomic data from zebrafish mutants is available through NCBI GEO (Accession # pending).

Funding statement: This study was supported by a pilot grant from the UC Davis MIND Institute Intellectual and Developmental Disabilities Research Center funded by NIH National Institute of Child Health and Human Development (P50HD103526), the NIH National Institute of Neurological Disorder and Stroke (R21NS128811), and the NIH Office of the Director and National Institute of Mental Health (DP2MH119424) to MYD. SSN is supported by the NIMH Autism Research Training Program T32 (MH073124) through the UC Davis MIND Institute; NAFM is supported by the NIGMS as a UC Davis Postbaccalaureate Research Education Program fellow (R25GM116690); GNL is supported by an NINDS Research Supplement to Promote Diversity in Health-Related Research (R21NS128811-01A1W1); NKH is supported by an NIGMS UC Davis eMCDB T32 (T32GM153586).

Conflict of interest disclosure: Authors have no conflicts of interest to report.

Clinical trials: This study involves no clinical trials. In accordance with the ICMJE and to be considered for review in Autism Research, the journal requires that clinical trials are prospectively registered in a publicly accessible database and clinical trial registration numbers are included in all papers that report their results. A clinical trial is defined as any research study that prospectively assigns human participants or groups to one or more interventions to evaluate the effects of those interventions on health-related biomedical or behavioral outcomes. The registry must be open to all registrants and managed by a not-for-profit group, and must have a mechanism to guarantee accuracy and validity of the information submitted. The registry must adhere to the ICMJE mandates described in the table found on their website. For more information regarding what Autism Research considers to be a clinical trial, please visit the Clinical Trial Registration section of our author guidelines.

Lay Summary

Autism (ASD) has become increasingly prevalent in children in recent years due to increasing awareness and improving diagnosis. While we know ASD is associated with hundreds of genes, there is much to learn about what genes are involved and how they contribute to its diverse presentation of traits and behaviors. By focusing on autistic individuals exhibiting enlarged brains (disproportionate megalencephaly), we identified new candidate genes possibly contributing to ASD and brain size. A autistic-patient-identified duplication of one gene in particular, *YTHDF2*, implicates a novel pathway related to RNA modifications with ASD and human brain size for the first time.

ABSTRACT

Among autistic individuals, a subphenotype of disproportionate megalencephaly (ASD-DM) seen at three years of age is associated with co-occurring intellectual disability and poorer prognoses later in life. However, many of the genes contributing to ASD-DM have yet to be delineated. In this study, we identified additional ASD-DM candidate genes with the aim to better define the genetic etiology of this subphenotype of autism. We expanded the previously studied sample size of ASD-DM individuals ten-fold by including probands from the Autism Phenome Project and Simons Simplex Collection, totaling 766 autistic individuals meeting the criteria for megalencephaly or macrocephaly and revealing 153 candidate ASD-DM genes harboring *de novo* protein-impacting variants. Our findings include thirteen high confidence autism genes and seven genes previously associated with DM. Five impacted genes have previously been associated with both autism and DM, including *CHD8* and *PTEN*. By performing functional network analysis, we expanded to additional candidate genes, including one previously implicated in ASD-DM (*PIK3CA*) as well as 184 additional genes previously implicated in ASD or DM alone. Using zebrafish as a model, we performed CRISPR gene editing to generate knockout animals for seven of the genes and assessed head-size and induced-seizure-activity differences. From this analysis, we identified significant morphological changes in zebrafish loss-of-function of two genes, *ythdf2* and *ryr3*. While zebrafish knockouts model haploinsufficiency of assayed genes, we identified a *de novo* tandem duplication impacting *YTHDF2* in an ASD-DM proband. Testing zebrafish overexpressing *YTHDF2* showed increased head and brain size matching that of the proband. Single-cell transcriptomes of *YTHDF2* gain-of-function larvae point to reduced expression of Fragile-X-syndrome-associated FMRP-target genes globally and in the developing brain, providing insight into the mechanism underlying autistic phenotypes. We additionally discovered a variant impacting a different m^6A-methylation reader, *YTHDC1*, in our ASD-DM cohort. Though we highlight only two cases to date, our study provides support for the m^6A-RNA methylation pathway as potentially contributing to this severe form of autism.

Keywords: Disproportionate megalencephaly, autism, genetics, zebrafish, YTHDF2, m^6A RNA methylation

INTRODUCTION

Autism is a group of neurodevelopmental traits characterized by difficulties with communication, social interactions, and behavioral challenges, prevalent in 1 out of 36 children in the United States [1]. Autism is highly heritable, with 50–90% of cases estimated to be driven by genetics alone [2–4]. Autism is also highly heterogeneous with large-scale whole exome sequencing (WES) of >63,000 autistic probands identifying 125 high confidence autism genes, with the predicted number of genes left to be discovered exceeding 1,000 [5–7]. In particular, leveraging genomic data from autism families—including parents and unaffected siblings—in the Simons Simplex Collection (SSC) [8] has identified coding *de novo* variants estimated to contribute to 30% of diagnoses [9–11]. More recently, whole genome sequencing (WGS) of SSC *de novo* noncoding mutations implicates risk in an additional 4.3% of autism cases [12,13]. Despite the combined efforts to sequence tens of thousands of genomes, known genes still only account for 5-20% of cases, and further work is required to fully elucidate genes and pathways contributing to autism etiology [5,6,14–22]. Combining *de novo* variation with autism sub-phenotyping has been used to address the heterogeneity of autism and identify susceptibility loci for comorbid phenotypes in an acute way [23].

Brain enlargement that is disproportionate to height, known as disproportionate megalencephaly (DM), is enriched in autistic probands with 15% of autistic boys falling under the DM subphenotype (ASD-DM) compared to 6% in typically developing (TD) boys [24]. This comorbidity is associated with more severe cognitive phenotypes, including lower IQ and language use, as well as higher rates of language regression [25–27]. This robust enrichment and distinct presentation support DM as a sub-phenotype of ASD, likely due to a shared genetic etiology between autism and DM. While a handful of genes have been associated with DM—including known autism genes impacting cell cycle and proliferation during embryonic development (*e.g.*, *CHD8* and *PTEN*)—mutations of known candidate genes make up only 3% of megalencephaly in autism probands. This leaves the genetic etiology of a majority of ASD-DM cases undiscovered [28–31]. A study using WES from 46 autistic families with macrocephaly (ASD-M)—defined as >2 standard deviations above the mean in head circumference for TD sex and age-matched children—successfully identified mutations in one novel and several known autism candidate genes [32], demonstrating the power of sub-phenotyping ASD-DM leading to genetic discoveries even for reduced sample size.

Zebrafish (*Danio rerio*) are an attractive model for studying neurodevelopmental traits given their rapid development, large number of progeny, transparent bodies, and that ~70% of gene orthologs are shared with humans [33–35]. Previous studies of known ASD-DM genes recapitulate macrocephaly and DM phenotypes in zebrafish knockdown and knockout experiments for *CHD8* and *KMT2E*, respectively [36,37]. This method of knocking down candidate ASD-M genes has also been used systematically to identify the contributing gene in the chromosome 16p11.2 locus in zebrafish [38]. Further, novel technologies such as the VAST BioImaging System allow for the rapid characterization of zebrafish knockout models through the generation of high resolution standardized images [39]. We recently demonstrated the utility of this approach by examining the knockdown of two genes associated with autism and microcephaly, *SLC7A5* and *SYNGAP1*, by assessing head-size phenotypes in CRISPR-generated zebrafish knockout line embryos at three and five days post fertilization (dpf) [40].

In this study, we leveraged high-coverage WGS data from two cohorts, 11 ASD-DM probands from the UC Davis MIND Institute Autism Phenome Project (APP) specifically identified using magnetic resonance imaging (MRI) data at around three years of age, and 755 ASD-M probands with head circumference data available from the SSC cohort. Together, this represents a >10-fold increase in probands compared to the previous largest study of increased head circumference associated genes in ASD [32]. Using this sub-phenotype-to-genotype analytic strategy, we identified candidate ASD-DM and ASD-M genes harboring *de novo* likely gene-disrupting (LGD) variants, including *CHD8* and *PTEN*, and subsequently functionally validated a subset of candidate genes using zebrafish. From this, we narrowed in on two genes impacting larval head size. Overexpression of *YTHDF2* results in macrocephaly in zebrafish following embryonic microinjection of mRNA, recapitulating the phenotype seen in the ASD-DM proband harboring a partial tandem duplication of the gene. Together our sub-phenotyping approach provides a powerful strategy to identify novel ASD-DM candidate genes and validate their role in brain development using a zebrafish model system.

METHODS

Megalencephaly and Macrocephaly Phenotypes

APP probands and determinations of megalencephaly were previously determined as part of the APP study [24]. Acquisition of MRI data for megalencephaly measurements were made during natural nocturnal sleep for children at study enrollment (time point 1), between the ages of 2 and 3.5 [41]. Blood collected during this time point was sequenced using the to 30X coverage WGS through a collaboration with MSSNG [42,43]. Raw data including FASTQ and VCF files can be accessed through the MSSNG access agreement: https://research.mss.ng.

Macrocephaly cases from the SSC were defined using a permissive cutoff of a head circumference >1.5 standard deviations (90%) above the mean of age matched controls [44]. Age matched TD head circumference data [45] and height data [46] from ages 4-17 were derived from publicly-available standards. For males in the SSC cohort 551/1601 (34%) met the criteria for macrocephaly, for females 108/245 (45%) met this criteria. We identified three types of macrocephaly: (1) somatic overgrowth (SO) with head circumference and height percentiles >90%; (2) disproportionate macrocephaly (DM) with height percentiles over head circumference percentile < 0.7; and (3) relative macrocephaly (RM) with height percentiles over head circumference percentile > 0.7.

Variant Annotation

Whole-genome sequencing, read mapping, and variant identification was performed for APP families as part of the MSSNG consortium [42,43]. *De novo* variants were identified in APP probands as those unique to the proband and absent from either parent via string matching (grep -Fvxf). We considered LGD variants as those predicted to lead a frameshift, nonsense, or splice site mutation. Rare variants were identified using dbSNP as those with a minor allele frequency (MAF) < 0.2% in all five 1000 Genomes ancestry-based populations [47,48]. The presence of all rare and *de novo* variants identified in the APP cohort were validated by visual inspection of sequencing data via the Integrated Genomics Viewer (IGV) [49].

Network and Ontology Analyses

Network analysis of known ASD-DM genes and candidate ASD-DM genes from this study were completed using the STRING database and visualized via Cytoscape [50,51]. Gene ontology (GO) analysis was completed for known ASD-DM genes and candidate ASD-DM genes as seed genes along with their top ten gene interactors determined using the STRING database, similar to previous studies [31]. Similar STRING database Molecular Function GO terminology were pooled. GO was completed using Database for Annotations, Visualization, and Integrated Discovery (DAVID) software [52]. Human genes were used as background for GO analyses.

Zebrafish CRISPR and mRNA models

Guide RNAs (gRNAs) were selected as having a CRISPRScan score of 35 or higher (Table S1) [53]. crRNA were synthesized by Integrated DNA Technologies. Injection mixes of ribonucleic protein (RNP) consisting of four pooled gRNA (annealed crRNA and tracrRNA) and SpCas9 Nuclease (New England Biolabs, M0386M) in order to achieve 90% knockdown efficiency [54], and were prepared as previously described [40]. Pooled gRNA (4 µM total concentration) were microinjected into single cell NHGRI-1 or transgenic zebrafish embryos to a volume of 0.5 nL/cell as previously described using a Pneumatic MPPI-2 Pressure Injector [55]. Scrambled injection RNP mix contained a single gRNA designed to have no target in the zebrafish genome. gRNA efficiencies were tested post-injection using pooled genomic extractions of four embryos and PCR amplification of targeted loci followed by 7.5% polyacrylamide gel visualization. These same amplicons were also subject to Illumina sequencing and the total alleles identified/quantified using the CrispRvariants R package (Figure S1, Table S1) [56].

Human mRNA was generated using cDNA plasmids (Horizon *YTHDF2*, MHS6278-202827242; *GMEB1*, MHS6278-202827172) [57] and prepared via the *in vitro* transcription kit mMESSAGE mMACHINE™ SP6 Transcription Kit (Thermo Fisher Scientific, AM1340). Mixes of 100 ng/µL mRNA and 0.05% phenol red were prepared, as previously described, and injected in single-cell zebrafish embryos at a volume of 0.5 nL/cell [58].

Zebrafish Morphometric Measurements

Dorsal and ventral images of 3 days post fertilization (dpf) embryos were obtained using the Union Biometrica VAST Bioimaging System with LP Sampler via the built-in camera and manufacturer settings [39]. Zebrafish features were identified and quantified from VAST using FishInspector software 2.0 [59]. FishInspector images were assessed for total area (contourDV_regionpropsArea), embryo length (contourDV_regionpropsLengthOfCentralLine), distance between the center of the eyes (YdistanceCenter_eye1DV_eye2DV), and telencephalon distance (YdistanceEdge_eye1DV_eye2DV). Statistical analysis was performed in R using the ggsignif package using the Wilcoxon test option [57,60].

Fluorescent images were acquired using the Andor Dragonfly High Speed Confocal Platform with the iXon Ultra camera. Human *YTHDF2* mRNA wasd microinjected Tg(HuC-eGFP) strain zebrafish, which harbor a green-fluorescent protein (GFP) fluorescent pan-neuronal marker, were bathed in 0.003% 1-phenyl-2-thiourea (PTU) in 10% Hank's saline between 20–24 pf for 24 hr (Fisher Scientific, 5001443999). At 3 dpf zebrafish embryos were embedded in 1% low melt agarose (Thermo Fisher Scientific, BP160-100) and imaged using a GFP filter.

Zebrafish Seizure Analysis

Zebrafish movement was recorded at 30 frames per second for 1 hr with no stimulation using ViewPoint's ZebraBox Technology per manufacturer recommendations [61]. Embryos were maintained at 37°C using a polystat water heating system. Movements were detected over one second intervals. Distance and time moved were analyzed using a custom R script and high speed events were quantified using a previously published MATLAB script [62].

Zebrafish RNA Extraction and RT-qPCR

Whole zebrafish larvae were collected at 3 dpf and stored in 50 µL RNALater at -80°C until RNA extraction. Three biological replicate samples were prepared for both *ythdf2* KO and scrambled control larvae, each containing 15 larvae, for pooled RNA extraction using an RNeasy Plus Mini kit (Qiagen). Briefly, larvae were resuspended in 350 µL of the buffer RLT and vortexed until homogenized. Instructions from the RNeasy Plus Mini kit were followed for DNA Removal using the gDNA Eliminator column. Samples were quantified using a Qubit BR kit and normalized to 4 ng/µL for RT-qPCR following the instructions from the NEB Luna kit.

Single-cell transcriptomics

Transcriptional differences across *YTHDF2* zebrafish models were assessed using single-cell (sc)RNA-seq. Cells were prepared from *ythdf2* knockout and SpCas-scrambled gRNA controls as well as *YTHDF2*-injected and eGFP-mRNA-injected controls. At 3 dpf, larval heads from each group were dissected after euthanasia in cold tricaine (0.025%), pooling 15 heads together per sample with three samples per group. Groups with low initial counts (*ythdf2* knockout and eGFP-mRNA) were repeated with an additional three samples. Cells from each sample were washed with 1 ml of cold 1x PBS twice and immediately incubated at 28°C in a mix of 480 µl of Trypsin-EDTA (0.25%) and 20 µl of Collagenase P (100 mg/ml) for a total of 15 min with gentle pipetting every 5 min to induce dissociation. To stop dissociation, 800 µl of cold DMEM with 10% FBS was mixed with each sample and immediately centrifuged at 4°C for 5 min at 700*g*. The supernatant was carefully removed from the cell pellet and cells were washed in cold 1x PBS and centrifuged at 4°C for 5 min at 700*g*, followed by another wash of cold DMEM with 10% FBS. Cells were then filtered into Eppendorf tubes using a P1000 pipette and a Flowmi 40 µm cell strainer (Sigma Aldrich, St. Louis, MO). 10 µl of sample was then mixed with 10 µl of trypan blue solution and counted using a Countess II (Thermo Fisher, Waltham, MA) to record cell viability. All samples processed were confirmed to show viability above 70%.

Cell fixation and library preparation were performed following the sci-RNA-seq3 protocol [63] using DSP/methanol. After the combinatorial indexing and PCR amplification steps, all wells were pooled together to ensure sufficient library yield before purification. The pooled libraries were then purified using AMPure XP beads to remove any remaining small fragments and primers. The quality and concentration of the libraries were assessed using a Bioanalyzer (Agilent Technologies, Santa Clara, CA) to ensure they met the required size distribution and concentration thresholds. Final libraries were size-selected using the Pippin HT system (Sage Science, Beverly, MA). The target range was set to 400-500 bp, with the smear cut between approximately 300-600 bp to ensure that only fragments within this desired range were included. The libraries were sequenced with paired-end read length of 150 bp using the Illumina NovaSeq 6000 platform.

FASTQ files were processed according to the sci-RNA-seq3 bioinformatic pipeline (https://github.com/JunyueC/sci-RNA-seq3_pipeline) and a comprehensive zebrafish transcriptome [64] was used to generate cell-by-gene matrices per sample. These matrices were processed into Seurat objects using *Seurat* v5.0.3 [65]. Cells with mitochondrial or ribosomal percentages above 5%, feature counts below 200 or over two standard deviations from the mean, and predicted doublets according to *DoubletFinder [66]* were removed from subsequent analyses. After quality-control filtering, an average of 1,126 cells per sample (4,785 cells per group) were obtained and normalized with the 5,000 most variable genes while regressing for ribosomal and mitochondrial percentages using *SCTransform*.

Samples were integrated using a reciprocal PCA reduction [65] and nearest-neighbor graphs were made using the first 30 principal components with the *FindNeighbors* function for subsequent clustering. Hierarchical clustering was initially performed using the Euclidean distance between all cells from principal component embeddings with the tree cut at k = 10. Broad marker genes were assigned using the *PrepSCTFindMarkers* and *FindAllMarkers* functions using the wilcox test option (parameters: *logfc.threshold*= 0.1, *min.pct*= 0.1, *return.thresh*= 0.01, *only.pos*= TRUE). Brain cells from a single broad cluster were isolated and hierarchical clustering was similarly repeated with the tree cut at k = 18. Cell clusters were defined using defined marker genes cross-referenced with larval zebrafish brain atlases [67,68] and the Zebrafish Information Network (ZFIN) [69].

For the differential gene expression analysis, cells from the *ythdf2* knockout and *YTHDF2*-injected groups were randomly sampled with respect to our original cluster distribution to match control cell counts (*downsampleSeurat*). Differentially-expressed genes (DEGs) were identified across all and a subset of brain cells, respectively, using the *FindMarkers* function with the wilcox test option (parameters: *logfc.threshold*= 0.1, *min.pct*= 0.01, *only.pos*= FALSE). A list of 842 high-confidence Fragile X Syndrome (FXS) protein (FMRP) targets [70] were converted to zebrafish orthologs using the g:Orth search from g:Profiler [71] to identify FMRP-target DEGs (adjusted p-value < 0.05) and assess enrichment using a Benjamini Hochberg (BH)-adjusted Fisher's exact test. All other FMRP-target genes expressed across both *ythdf2* knockout and *YTHDF2* mRNA conditions in at least 0.01 percent of cells were selected for subsequent analysis (n=675). *scCustomize [72]* and *dittoSeq [73]* were used for figure creation. *Nebulosa [74]* was used to visualize joint expression from multiple FMRP-DEGs using a kernel gene-weighted density estimation.

RESULTS

ASD-DM Candidate Gene Discovery

ASD-DM individuals were recruited through the UC Davis APP—a longitudinal study focused on the identification of ASD-subphenotypes [24,75,76]. Using MRI data from the study entry time point (2–3½ years of age) [75], we selected 11 individuals in the APP cohort that met the criteria for ASD-DM, defined as a cerebral volume to height ratio >1.5 standard deviations above the mean compared to TD age-matched controls. Through a collaboration with MSSNG [17,43], WGS and variant identification/annotation was performed for the autistic probands and a subset of family members, for which we also had blood specimens, including six trios and five non-trio probands yielding over 200 thousand variants. From this, we identified two exonic, *de novo*, LGD variants from trio families,

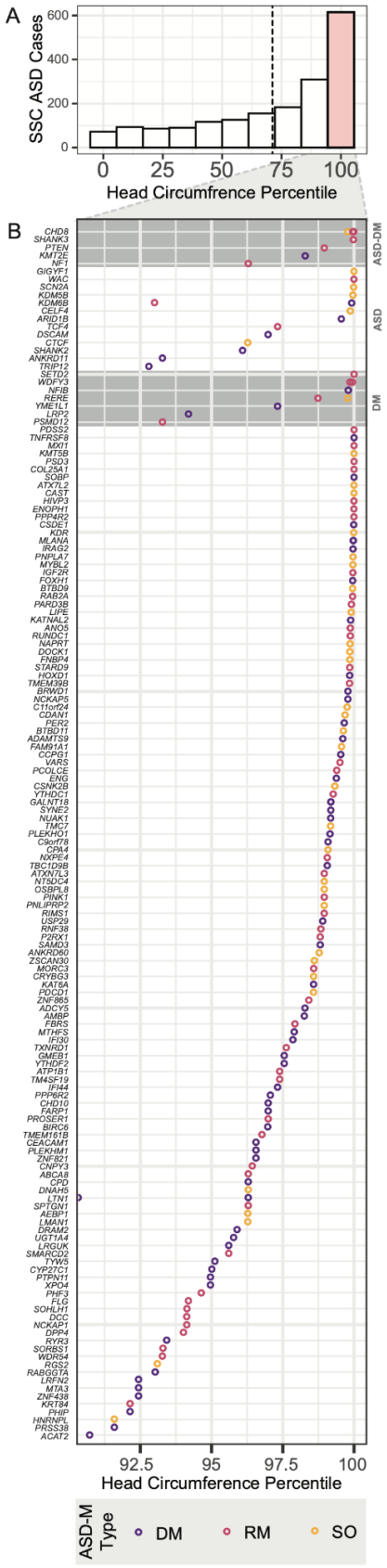

including one single-nucleotide variant (SNV) splice-site variant impacting *RYR3* and one 109-kbp duplication of *YTHDF2* and *GMEB1*. From the five individuals with no parental data, we identified a proband harboring a chromosome 1q21.1 microduplication, a copy-number variant (CNV) previously associated with ASD-DM [77], and a single proband with variants in *CHD8* and *KMT2E* [78]. An additional ten variants were found in non-trio proband data to be exonic, LGD, and rare (not previously recorded in dbSNP) [79]. Of these, three impacted genes have SFARI scores of 3S or above (*KMT2E*, *RPS6KA5*, and *TTN*), an additional three genes have known neuronal functions (*DMBT1*, *IARS2*, *FGF12*), and one gene was found recurrently carrying variants in two probands (*SPANXN4*) [80].

SSC consists of trios and quads of simplex autism families with accompanying genetic and phenotypic information. Due to the lack of MRI data for SSC participants, we used ASD-M as a proxy for ASD-DM. SSC head circumference and age data was used to determine ASD-M status (head circumference >1.5 standard deviations above the mean for typically developing sex and age-matched children) for 755 of 1,846 SSC probands (40%) [8] (Table S2, Figure S2). Considering only SNVs and indels, ASD-M *de novo* LGD variants were identified from published results [12], overlapping a total of 150 genes (Figure 1, Table S3). Of note, five genes were found recurrently mutated in ASD-M, including *GALNT18*, *KDM6B*, *LTN1*, *RERE*, and *WDFY3*, as well as *CHD8*, which was disrupted in three probands.

Figure 1. Macrocephaly level of candidate ASD-DM and ASD-M genes. (A) A histogram representing the number of SSC probands v. head circumference percentiles shows a skew towards larger head-sizes compared to age and sex-matched typically developing children. The red bar designates those meeting the criteria for macrocephaly. The dashed line represents the distribution mean. **(B)** ASD-DM and ASD-M genes listed by their identified proband's head circumference percentiles show genes previously associated with ASD-DM (first gray quadrant) are more likely to be associated with a higher head circumference percentiles than genes previously associated with autism (second white quadrant) and DM (third gray quadrant) alone. Color represents the macrocephaly type. DM, disproportionate macrocephaly; RM, relative macrocephaly; SO, somatic overgrowth.

In total, we identified 153 genes containing a LGD variant across the APP ASD-DM and SSC ASD-M datasets. Rates of harboring a LGD *de novo* variant in ASD-DM probands were in line with previous predictions (19.4%) and nominally enriched compared to TD SSC siblings (16.5%), though not statistically significant (chi-squared p-value = 0.1) [9,32]. Over a third of identified candidate genes (53/153) had a pLI score of > 0.9, suggesting intolerance to variation [81] (Table S3). Examining *de novo* missense variants, which were previously shown to exhibit overall enrichments in affected probands versus unaffected siblings [82,83], we did not observe an enrichment in our LGD candidate genes in ASD-M probands compared to TD siblings of ASD-M probands, ASD-without-macrocephaly (ASD-N) probands, and siblings of ASD-N probands (Student's T-test, p-values = 0.16, 0.29, 0.76).

ASD-DM Candidate Gene Discovery Using Network Analysis

Identifying shared patterns of molecular functions and ontologies of impacted ASD-DM genes may point to additional gene candidates. Due to the highly heterogeneous nature of ASD, this type of analysis expands our ability to identify disrupted biological mechanisms and spatio-temporal expression patterns implicated in autism [31]. Here, we used as seeds 166 previously-known and identified-in-this-study ASD-DM genes to identify active interactions using the STRING database (Figure 2) [32,50]. This analysis uncovered ontology groups enriched in our dataset previously reported for ASD, including proteins involved in histone modification and chromatin organization, transcription factors, cell signaling (e.g., SMAD and E-box binding), functions key to neuronal activity (e.g., sodium and calcium ion transport and glutamate receptor binding), cell adhesion and cytoskeletal proteins, and mRNA binding (Table S4) [84–87]. Out of our original ASD-DM candidate seed genes 41.5% (69/166) fall under one of these ontologies.

We next used the Database for Annotations, Visualization, and Integrated Discovery (DAVID) to identify unique ontologies enriched in the 166 known and candidate ASD-DM genes compared to ontologies enriched in SSC ASD-N proband LGD genes, versus genes previously associated with DM [52,88]. While there are many commonalities between the subphenotype and ASD-N, including chromatin remodeler, ASD-DM is uniquely enriched for terms such as intellectual disability, synapse assembly and long-term synaptic depression, histone methyltransferase activity, cytoskeletal structure (spectrin repeats) (Table S4). Notably, unlike ASD-N (*GRB10*, *PPP2R5D*, *RICTOR*, and *TSC1*), there was no enrichment in LGD variants impacting genes related to the MTOR pathway for ASD-DM (*NF1* and *PTEN*) [89].

We next sought to identify putative additional candidate ASD-DM genes by expanding our network to include the top ten interactors for each ASD-DM seed gene (Table S5). This list of top ten interactors included genes defined by STRING as having known protein interactions, shared homology, and co-expression patterns [50]. Of the ASD-DM candidate gene interactors, 28% (518/1826) fall under one of the ontologies found in our ASD-DM network. Interestingly, one of these genes has previously been associated with both autism and DM individually, *PIK3CA* (Table S6). *PIK3CA* functions as a catalytic subunit of the mTOR pathway and has previously been found to be associated with developmental delay and DM, including one individual diagnosed with autism [90].

In this ASD-DM interactor set, twenty genes are high-confidence autism genes not previously associated with DM (*ANK2*, *ASXL3*, *CTNNB1*, *CUL3*, *DLG4*, *DYRK1A*, *GNAI1*, *GRIN2B*, *KCNMA1, KMT2A*, *NCOA1*, *NIPBL*, *NRXN1*, *PHF12*, *POGZ*, *PPP1R9B*, *SIN3A, SMARCC2*, *TBL1XR1*, *UBR1*). Eighteen

additional genes from this interactor set have been implicated in DM and implicated as SFARI putative autism candidate genes (*ANK3*, *CHD2*, *CHD3*, *FRMPD4*, *HCFC1*, *HDAC4*, *HRAS*, HUWE1, *PAK1*, *PIK3R2*, *RAC1*, *SETD1A*, *SLC25A1*, *SMAD4*, *TBL1X*, *TRIO*, *USP7*, and *USP9X*), and 184 more have been implicated in DM or have a SFARI score. Especially promising are the 21 genes that contain missense variants in the SSC ASD-M probands, but not in ASD-N probands or their TD siblings, including *ABI2*, *ANK3*, *SRC*, *SRCAP*, *ATP12A*, *BAIAP2*, *CHD13*, *CH815*, *FGG*, *JUP*, *KDM2A*, *KIF20A*, *MAPK8*, *PDGFRB*, *RING1*, *SCN4A*, *SHANK1*, *SMC3*, *TCF3*, *WDR5*, *ZC3H3*. Together, network analysis and ontology point to these genes as promising ASD-DM candidate genes going forward.

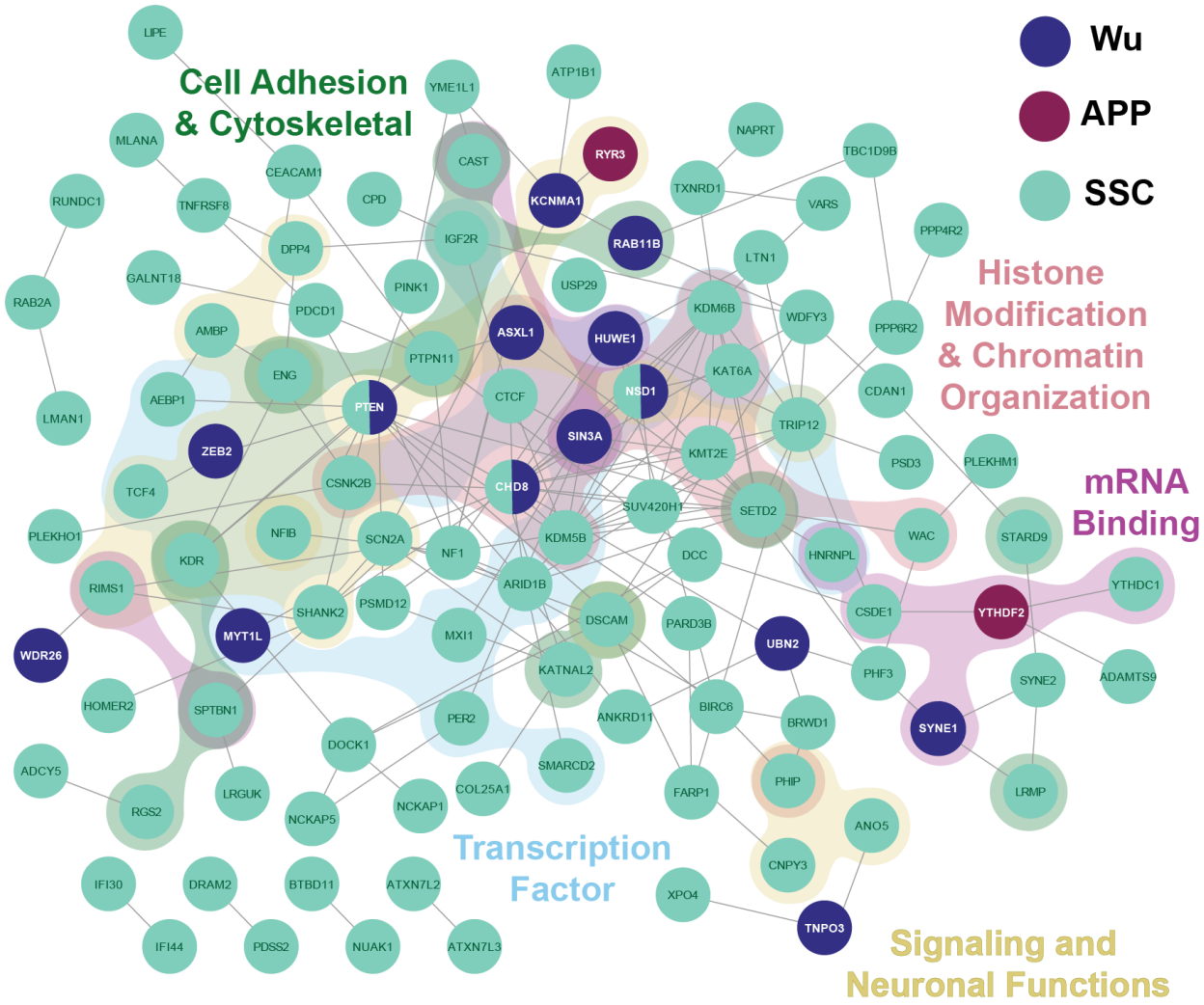

Figure 2. Network analysis and gene ontology of ASD-DM candidate genes. ASD-DM candidate genes from SSC (teal), APP (purple), and Wu (navy) probands are connected in a network via active interactions as determined by STRING [50]. Background colors represent shared GO molecular functions. Disconnected gene nodes are not included.

Validation of Candidate Genes in a Zebrafish Model System

In order to determine if our candidate ASD-DM genes contribute to a head-size phenotype, we tested seven by CRISPR knockout in zebrafish (Figures S1 & S3). We focused our analysis on the previously unstudied candidates from the APP cohort, including the three genes impacted by *de novo* variants, *RYR3*, *GMEB1*, and *YTHDF2*. It is known that ~20% of zebrafish genes conserved with humans are also duplicated; we therefore prioritized candidate ASD-DM genes with only a single ortholog in zebrafish (*IARS2* and *RPS6KA*) [91]. Additionally, we included two genes from the SSC ASD-M cohort, *CHD8*, for which CRISPR F_0 mosaic knockouts have previously been shown to lead to increased interorbital distance in zebrafish embryos [36], and *FAM91A1*, a gene previously not implicated in ASD. Finally, as controls, we included three genes found in SSC ASD-N probands for which we do not expect to see a head-size phenotype—*HEPACAM2*, *PAX5*, and *SCP2A*.

We generated CRISPR knockout F_0 embryos (or "crispants") by microinjection of four gRNAs targeting exonic regions of each candidate gene. This approach has been shown to result in near complete mosaic knockout of genes with little off-target effects [32,40,92]. We then quantified morphometric features in 3 dpf larval crispants, including embryo area, body length, and distance between the center of the eyes (as a proxy for head size). From this analysis, we identified two genes (*ryr3* and *ythdf2*) showing significant head-size differences in zebrafish knockout embryos compared to negative scrambled injection controls (Wilcoxon T-test p-values < 0.01) (Figure 3). In both cases, crispant embryos exhibited reduced head size consistent with microcephaly, with *ryr3* showing a mean reduction of 3.3% and *ythdf2* showing a mean reduction of 3.8%. *RYR3* encodes a ryanodine receptor responsible for calcium transport in muscle and brain tissue, and *YTHDF2* encodes for part of the m^6A-mRNA degradation complex [93,94]. Though *ythdf2* also displayed a reduction of body area and length, this size difference did not appear to be due to overall developmental delay, measured by head-trunk angle (Figure S4). This was in contrast to a previous study of a morpholino *ythdf2* zebrafish knockout, which noted an overall delay in development as well as potential compensation of m6A-mRNA clearance activity [95]. Only genes harboring known *de novo* variants from the ASD-DM APP cohort exhibited head-size phenotypes, though we did not observe any morphometric differences of our F_0 mosaic *chd8* crispant, counter to published results in stable lines and using morpholinos [35,36,96].

As increased prevalence of seizures is highly enriched in autism [97], we assessed our knockout embryos for increased susceptibility to drug-induced seizures [98] by treating them with GABA antagonist pentylenetetrazole (PTZ; 5 mM) at 5 dpf [40,99]. High-speed events, corresponding to seizure-like movements, were recorded using motion tracking [61] and quantified [62] (Figure 3). This analysis revealed three crispant models associated with increased high speed events versus scrambled controls, *fam91a1*, *gmeb1*, and *hepacam2*. Of note, *HEPACAM2,* an immunoglobulin gene responsible for cell adhesion, showed the highest fold increase in high speed events compared to controls in our zebrafish assay. This gene falls within the human chromosome 7q21.3 microdeletion syndrome region associated with myoclonic seizures in humans [32,100]. Mutations in *FAM91A1*, responsible for Golgi protein trafficking, have been linked to dysregulated electrophysiological brain activity [101,102], while *GMEB1*, a caspase activation and apoptosis inhibitor, has no previous connections with seizures.

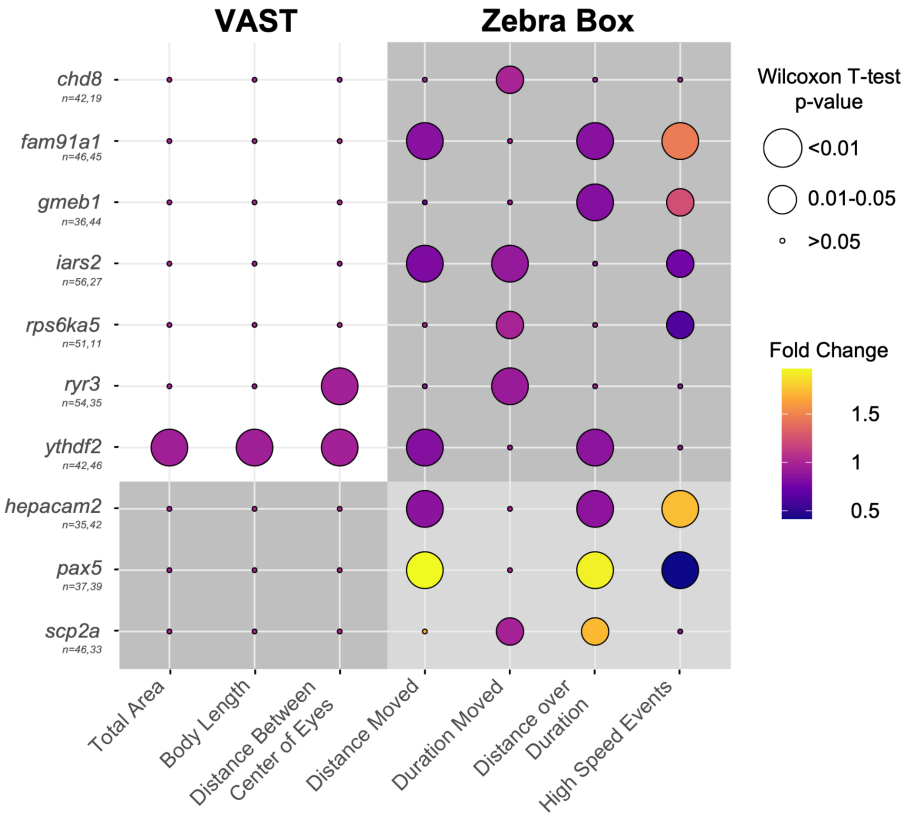

Figure 3. **Zebrafish CRISPR knockout embryos for the rapid validation of ASD-DM genes.** Phenotyping knockout zebrafish morphometric measurements using the VAST BioImaging System, we identified *ryr3* and *ythdf2* as having reduced head size compared to a negative scrambled control. Seizure-like activity in the presence of PTZ was assessed using ZebraBox video motion tracking. Circle size represents the inverse Wilcoxon T-test p-value. Circle color represents the fold change compared to a negative scrambled control.

YTHDF2 in ASD-DM

Based on the findings that knockout crispants targeting *ythdf2* exhibited microcephaly and *gmeb1* displayed increased seizure activity, we sought to better characterize the *de novo* 109-kbp duplication identified in an APP ASD-DM proband. To begin, we validated the duplication existed in the proband but not parents using sequence read depth (QuicK-mer2) [49,103] (Figure 4A). Split reads falling at the identified breakpoints indicated that the duplication, harboring the entire *GMEB1* gene and the first five of six exons of *YTHDF2*, inserted in tandem at the 3' untranslated region (UTR) of the noncoding divergent transcript of *TAF12*, directly upstream of *GMEB1* (Figure 4B and C). Using available microarray data produced from mRNA derived from whole venous blood, we found that both *GMEB1* and *YTHDF2* exhibited increased expression > 3 standard deviations from the mean in the APP proband harboring the duplication compared to other APP participants [104].

GMEB1 is an auxiliary factor in parvovirus replication known to inhibit apoptosis in neurons and previously associated with schizophrenia [105,106], and *YTHDF2* is a member of the m^6A-containing mRNA degradation complex known to be downregulated in neuronal fate determination [94], making both of these attractive potential ASD-DM candidate genes. Based on their known functions, duplication of either gene could plausibly result in neurodevelopmental effects. Therefore, we modeled increased

expression of *YTHDF2* and *GMEB1* by microinjecting human *in vitro* transcribed mRNA into single-cell stage zebrafish embryos. We then assessed morphometric features of 'overexpression' zebrafish embryos at 3 dpf (Figure 4D). For *YTHDF2*, we observed increased telencephalon length compared to a dye injected negative control consistent with increased head size but no significant differences to body area or length, matching the proband phenotype. We did not observe any difference in head size for the *GMEB1*-injected larvae (Figure 4D). To verify the increased head size was a result of an enlarged brain, we repeated the experiment in the zebrafish transgenic line HuC-GFP [107], which harbors a green-fluorescent protein (GFP) pan-neuronal marker (Figure 4E and F). These embryos displayed brain size differences, with knockout embryos showing significantly reduced midbrain, and mRNA injected 'overexpression' embryos exhibiting significantly increased midbrain and forebrain compared to injection controls. Together, the knockout and mRNA injected zebrafish provide evidence that increased dosage of *YTHDF2* is associated with DM while its loss leads to microcephaly.

Exploring the *YTHDF2* models further, we verified haploinsufficiency in our crispant larvae, showing a significant ~0.37 fold change (FC) in *ythdf2* expression versus scrambled controls through quantitative RT-PCR analysis (p-value < 0.001; Figure S5). To better characterize *ythdf2* neurodevelopmental phenotypes, we next performed sci-RNA-seq [108] of knockout and overexpression models at 3 dpf, profiling 19,141 single cells from mechanically-isolated heads (average of 4,785 cells per group or 1,126 cells per biological replicate; Table S7). Using known marker genes, we identified nine broad clusters and observed widespread localization of *ythdf2* across cell types (Figure 4G, Figure S6A). This agrees with its reported general expression in humans [109] and zebrafish [110,111] (Figure S7), which begins early in development at 3 hours post fertilization [112].

Differential gene expression analysis across all cells (with counts balanced relative to controls, see Methods) revealed 131 DEGs in our *ythdf2* knockout and 33 DEGs in *YTHDF2* mRNA overexpression model versus respective controls (adjusted p-value cutoff = 0.05, $\log_2$FCcutoff = 0.1; Figure 4H, Table S8). While our ASD-DM network did not show associations with DEGs in our models (n=1826; Figure 2), we did observe a significant enrichment of high-confidence Fragile X Syndrome (FXS) protein (FMRP) targets amongst our DEGs (3.6% expected vs 7.2% observed enrichment of DEGs considering 842 target genes; Fisher's exact test BH-adjusted *p*-value = 0.008; Figure 4H). This list includes genes with known functions in neurodevelopment, including ncam1a, cux1a, unc5a, tbc1d9, ncam1a, camta1a, magi2b, syt1a, sv2bc, stxbp1b.,

Recent studies have suggested that FMRP and YTHDF2 compete for binding to m^6A-methylated RNA targets impacting their stability [70,113]. Overlapping expression of the 15 FMRP-target DEGs through joint density profiles shows strongest expression across brain cells. Further subtyping the brain cluster into 18 cell types (Figure 4I, Figure S6B) highlights forebrain and midbrain neurons. Considering all FMRP-target genes, we observed significantly reduced expression in *YTHDF2* mRNA compared with *ythdf2* knockout larvae considering all cells (*p*-value = 2.4×10^{-7}, Figure 4H) and only brain cells (*p*-value = 2.4×10^{-7}, Figure S6C). These combined results are consistent with previous studies implicating YTHDF2 as preferentially binding to FMRP target genes resulting in mRNA degradation and global downregulation.

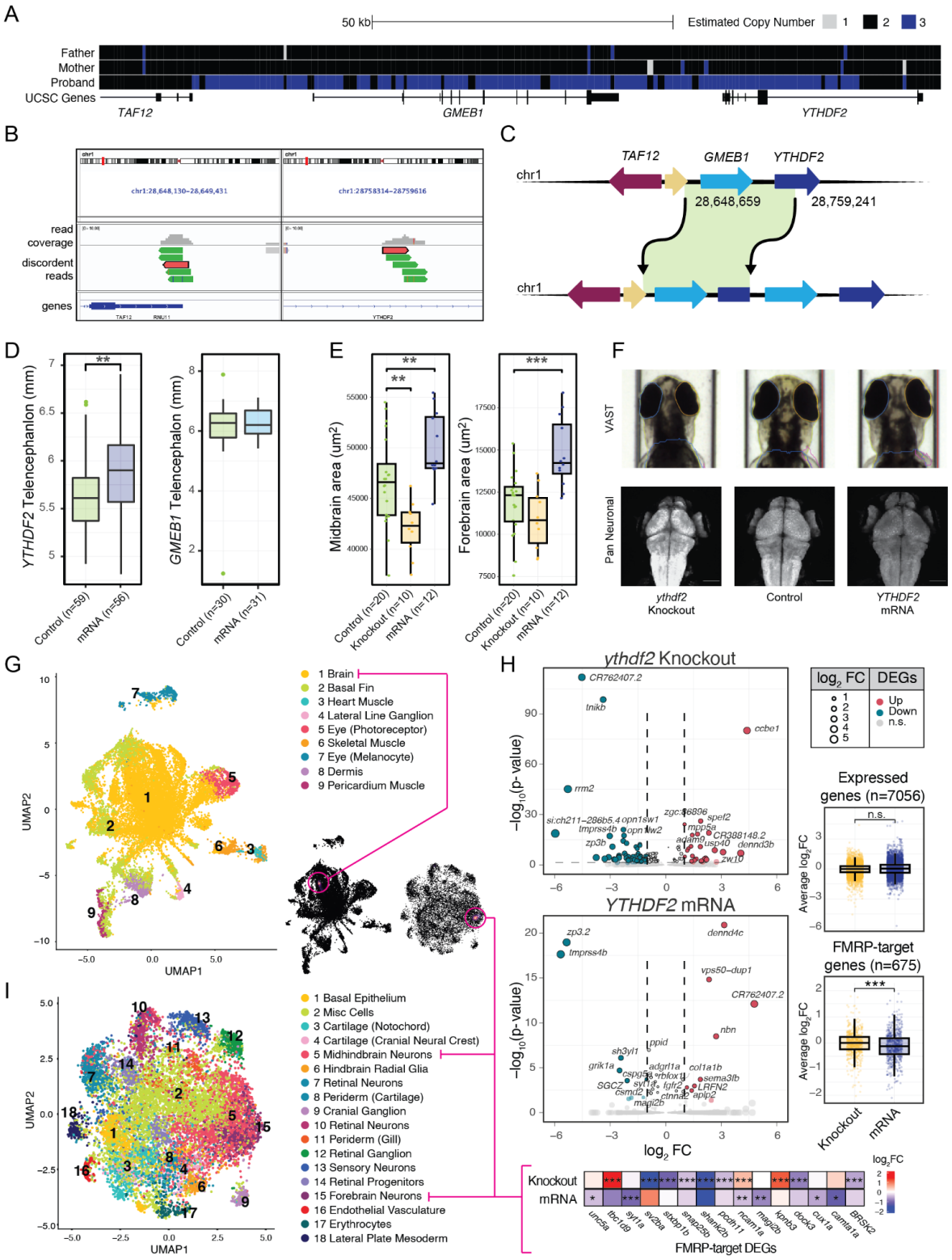

Figure 4. Disrupting *ythdf2* in zebrafish is associated with head and brain size phenotypes. (**A**) Copy-number-estimate plot (QuickMer2) using sequencing data from the APP proband harboring a *de novo* duplication a 109-kb duplication on chromosome 1 compared to their parents harboring two diploid copies. (**B**) IGV plot showing discordant reads in the APP proband supporting a tandem duplication. (**C**) An illustration of the tandem duplication on chromosome 1 in an APP proband encompassing *GMEB1* and all but the last exon of *YTHDF2*. (**D**) Head size of

mRNA injected zebrafish, estimated via telencephalon measurement, are significantly increased after *YTHDF2* mRNA microinjection into zebrafish embryos (Wilcoxon T-test p-value = 0.0013), and unchanged in *GMEB1* mRNA injected embryos at 3 dpf (Wilcoxon T-test p-value = 0.8). (**E**) Knockout and mRNA injected zebrafish harboring a pan neuronal marker reveal brain size differences at 3 dpf. Knockout embryos show significantly decreased midbrain volume (Wilcoxon T-test, p-value = 0.003). mRNA injected embryos show both significantly increased midbrain (Wilcoxon T-test, p-value = 0.007) and forebrain (Wilcoxon T-test, p-value = 0.0005). (**F**) Representative control, knockout, and mRNA injected zebrafish images from wildtype embryos imaged with the VAST bioimaging system and HuC embryos harboring a pan neuronal fluorescent marker. Scale bar is 100 μm. (**G**) Hierarchical clustering of 19,141 cells across all conditions into 9 broad cell types based on the expression of gene markers. Joint kernel density estimation was calculated from all 15 FMRP-target DEGs (Nebulosa) highlighting higher expression within a sub-type of brain cells. (**H)** Volcano plots showing DEGs across all cell-types within *ythdf2* knockout (top left) and *YTHDF2* mRNA overexpression (bottom left) conditions relative to controls. DEGs with absolute $\log_2$`FC ≥ 1 and p-adj ≤ 0.05 are colored (upregulated as red, downregulated as blue). Average` $\log_2$FC across all expressed genes shows no significant difference between knockout and overexpression groups (top right), while average $\log_2$FC across orthologs of all 675 FMRP-target genes expressed in both groups shows a reduction in overexpression relative to knockout. (**I**) Hierarchical sub-clustering of 12,066 brain cells across all conditions into 18 cell types based on the expression of gene markers. Joint kernel density estimation plot highlights higher FMRP-target DEGs expression within forebrain and midhindbrain neurons. Average $\log_2$FC for all 15 genes across knockout and overexpression with respect to controls is shown. All *p*-values in this figure are represented as: <0.05*, <0.01**, <0.001***.

DISCUSSION

The autism sub-phenotype ASD-DM, which occurs in approximately 15% of autistic boys, is associated with lower language ability at age three and slower gains in IQ across early childhood resulting in a higher proportion with IQs in the range of intellectual disability by age six [24]. Clues at the underlying etiology of ASD-DM can be found in high-confidence genes such as *CHD8*, a chromatin remodeler important in early brain development [36,114], and *PTEN*, a tumor suppressor gene that functions in cell proliferation [44]. While variants impacting these two genes alone are estimated to contribute to up to 15% of all ASD-M cases [32], a majority of cases remain unsolved. Here, we examined the genomes of 766 ASD-DM and ASD-M trios and quads from the APP and SSC cohorts to identify 153 ASD-DM candidate genes containing *de novo* LGD variants. Ontologies of affected genes largely matched those previously implicated in ASD [115].

When compared with genes implicated in ASD-N and DM-alone, functions related to synapse assembly and long-term synaptic depression, histone methyltransferase activity, cytoskeletal structure stand out in ASD-DM alone (Table S4). To further disentangle mechanisms shared and unique to ASD-DM, we collectively categorized the identified genes from our study and previously published [32] as high-confidence ASD-DM (n=5), ASD-N (n=13), and DM-alone (n=7), as well as those with uncertain disease relevance (n=128) (Table 1). Perhaps unsurprisingly, 16% of high-confidence disease risk genes exhibit recurrence in our cohort, including *CHD8* with three probands affected, while only two genes (*GALNT18* and *LTN1*) in the uncertain "Other" category. These latter genes represent compelling ASD-DM risk candidates, with *GALNT18* (Polypeptide N-Acetylgalactosaminyltransferase 18) functioning in O-linked glycosylation, and *LTN1* (Listerin E3 Ubiquitin Protein Ligase) encoding a RING-finger protein and E3 ubiquitin ligase [36,116–120].

Table 1. Candidate ASD-DM genes.

Category	Candidate Genes
ASD-DM (n=5)	*CHD8* [3], *KMT2E* [ASD-N], *NF1* [DP], *PTEN* [DP], *SHANK3* [DP]
ASD (n=13)	*ANKRD11* [ASD-N], *ARID1B* [ASD-N], *CELF4*, *CTCF*, *DSCAM* [DP, ASD-N], *GIGYF1* [DP, ASD-N], *KDM5B* [DP], *KDM6B* [2, DP], *SCN2A* [DP, ASD-N], *SHANK2*, *TCF4* [DP], *TRIP12*, *WAC* [DP, ASD-N]
DM (n=7)	*LRP2* [DP], *NFIB* [NO], *PSMD12*, *RERE* [2,DP], *SETD2*, *WDFY3* [2], *YME1L1* [DP]
Other (n=128)	*ABCA8* [DP], *ACAT2*, *ADAMTS9*, *ADCY5* [ASD-N], *AEBP1* [DP], *AMBP*, *ANKRD60* [NO], *ANO5* [DP], *ATP1B1* [DP, ASD-N], *ATXN7L2* [DP], *ATXN7L3*, *BIRC6*, *BRWD1*, *BTBD11* [DP], *BTBD9*, *C11orf24*, *C9orf78*, *CAST*, *CCPG1*, *CDAN1*, *CDH10* [DP], *CEACAM1*, *CNPY3*, *COL25A1*, *CPA4* [DP], *CPD* [DP], *CRYBG3* [NO], *CSDE1*, *CSNK2B*, *CYP27C1*, *DCC*, *DNAH5*, *DOCK1*, *DPP4*, *DRAM2* [DP], *ENG* [DP], *ENOPH1*, *FAM91A1*, *FARP1*, *FBRS*, *FLG* [NO], *FNBP4*, *FOXH1*, *GALNT18* [2,DP], *GMEB1*, *HIVEP3* [DP], *HNRNPL* [DP], *HOXD1*, *IFI30* [DP], *IFI44* [DP], *IGF2R*, *KAT6A*, *KATNAL2* [DP], *KDR*, *KMT5B*, *KRT84* [DP], *LIPE* [DP], *LMAN1*, *LRFN2* [DP], *LRGUK*, *LRMP*, *LTN1* [2], *MLANA* [,NO], *MORC3* [DP], *MTA3*, *MTHFS* [DP], *MXI1*, *MYBL2* [DP], *NAPRT*, *NCKAP1* [ASD-N], *NCKAP5* [NO], *NT5DC4*, *NUAK1* [DP], *NXPE4* [DP], *OSBPL8*, *P2RX1*, *PARD3B* [DP], *PCOLCE* [DP], *PDCD1* [NO], *PDSS2*, *PER2*, *PHF3*, *PHIP*, *PINK1**, *PLEKHM1*, *PLEKHO1* [DP], *PNLIPRP2* [NO], *PNPLA7* [DP], *PPP4R2* [DP], *PPP6R2* [DP], *PROSER1*, *PRSS38* [NO], *PSD3*, *PTPN11** [,DP], *RAB2A*, *RABGGTA*, *RGS2*, *RIMS1* [DP, ASD-N], *RNF38*, *RUNDC1*, *RYR3*, *SAMD3* [NO], *SMARCD2*, *SOBP* [DP], *SOHLH1* [NO], *SORBS1*, *SPTBN1*, *STARD9*, *SYNE2* [DP], *TBC1D9B*, *TM4SF19* [DP], *TMC7* [NO], *TMEM161B*, *TMEM39B*, *TNFRSF8* [NO], *TXNRD1*, *TYW5*, *UGT1A4* [DP], *USP29* [DP], *VARS**, *WDR54*, *XPO4*, *YTHDC1*, *YTHDF2*, *ZNF438*, *ZNF821*, *ZNF865*, *ZSCAN30* [NO]

[2,3] Number of occurrences in cohort, if more than 1

[DP] Duplicate paralogs in zebrafish

[NO] No ortholog in zebrafish

[ASD-N] LoF variant in ASD-N SSC proband

As 43% of *de novo* LGD variants in probands have been estimated to contribute to an autism diagnosis, we anticipate that many of the genes identified in this study contribute to ASD-DM or autism in general [9]. Nevertheless, only a single variant was discovered for a majority of candidates limiting our ability to narrow in on true causal genes. As a result, we functionally tested seven genes using zebrafish coupled with CRISPR knockout and discovered two resulting in reduced head sizes in 3 dpf larvae: *ryr3* and *ythdf2*. In the case of the *ryr3* knockout, our findings of microcephaly are counter to those observed in the autistic proband with an identified LGD splice-site variant of *RYR3* resulting in DM (chr15:33634585; G>T). Further experimentation delineating the molecular mechanisms of the variant will be necessary in order to determine if reduced head size in knockout zebrafish larvae might be due to splice alterations of *RYR3* leading to gain-of-function in the patient, or intra-species differences in ortholog functions between humans and zebrafish.

To appropriately model the identified patient *YTHDF2* duplication, for which we hypothesize gene gain-of-function effects, we overexpressed human *YTHDF2* in zebrafish, recapitulating both increased head and brain sizes (Figure 4). To our knowledge, *YTHDF2* gain-of-function has not previously been characterized *in vivo*. Alternatively, published knockout models of the gene in mice [121] and zebrafish [95], using TALENs and morpholinos that target maternal *ythdf2* transcripts, exhibit severe phenotypes and large rates of embryonic death. Generally, the gene exhibits considerable functional constraint between species (e.g., 95% homology with mouse and 72% with zebrafish) and across hundreds of thousands of sequenced humans, with a significant depletion of LGD SNVs discovered to date (gnomAD

pLI score of 1, LOUEF score 0.132) [81]. Further, assessment of individuals from the 1000 Genomes Project (n=2,504), SSC families (n=9,068), and gnomAD (n=464,297) did not identify any CNVs impacting *YTHDF2*. Combined, these results highlight the rarity of the 109-kbp duplication impacting *YTHDF2*, identified in a single ASD-DM proband, and suggests that variants impacting this gene could plausibly lead to disease pathogenicity and/or lethality.

In addition to its high conservation, *YTHDF2* is a feasible contributor to ASD-DM based on its previously-implicated functions in neurodevelopment [121,122]. The encoded protein exists in the cytoplasm where it designates m^6A-labeled RNA for degradation [123] through the recruitment of protein complexes that deadenylate and de-cap mRNA [123,124]. It has over 3,000 target transcripts, including some previously associated with ASD such as *CREBBP* [94]. Studies using induced pluripotent stem cells show that the gene is required for neuronal fate determination, with *YTHDF2* knockdown leading to delayed mitotic entry [125,126] and inhibited pluripotency [127]. Conditional knockout mouse models of *Ythdf2* exhibit decreased cortical thickness as a result of reduced neurogenesis in early development [121]. Together, these results suggest that *YTHDF2* duplication leads to delayed neuronal fate determination, resulting in an overabundance of neuronal progenitor stem cells followed by increased neurogenesis.

While functions of *YTHDF2* in cell cycle and proliferation mechanistically associate it with brain-size phenotypes, evidence of its interactions with mRNA-binding FMRP provide plausible connections with ASD. FXS, caused by loss of FMRP function, represents the most common single-gene cause of ASD, accounting for 2–6% of diagnosed cases [128]. Interestingly, FXS has a similar increased prevalence of macrocephaly as in ASD [129,130]. Several studies have shown FMRP preferentially binds modified RNAs through recognition of m^6A consensus motifs resulting in protection of transcripts from YTHDF2-mediated degradation [131–133], possibly through direct interactions of the two proteins. This is evident in mouse neuroblastoma cells, where the loss of Fmrp is associated with reduced m^6A-modified transcripts, while knockdown of *Ythdf2* leads to increased stability and longer half lives of modified RNAs [131].

In our transcriptomic analysis of *YTHDF*2 zebrafish models, we found significant enrichment of FMRP-target DEGs when considering both knockout and mRNA-overexpression larvae, with several genes exhibiting opposing effects in knockout versus overexpression (Figure 4H). One example is *ncam1* (Neural adhesion molecule 1), where we observed significant upregulation in *ythdf2*-knockout and downregulation in *YTHDF2*-mRNA larvae; this is in line with several studies in humans connecting depressed *NCAM1* expression with ASD [134–137]. Further, we show that overexpressing *YTHDF2* in zebrafish is associated with decreased expression of FMRP-target genes across all cells and in the brain (Figure S6), likely due to increased degradation of m^6A-modified mRNAs. Based on these collective findings, we propose a model in which *YTHDF2* loss-of-function results in microcephaly and possibly mortality, by increasing stability of m^6A-labeled RNAs resulting in extended cell-cycle progression and a reduction in neurogenesis (Figure 5). Alternatively, *YTHDF2* gain-of-function results in increased degradation of m^6A-modified transcripts, possibly contributing to megalencephaly through increased neurogenesis and ASD through haploinsufficiency of FMRP-target genes [138].

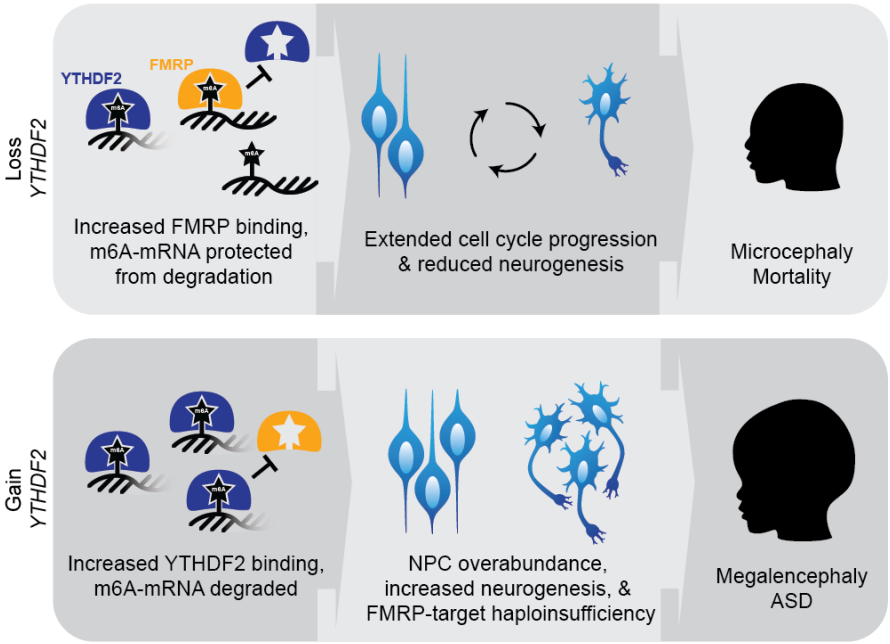

Figure 5. A potential role for *YTHDF2* in ASD-DM. Proposed model of *YTHDF2* loss- or gain-of-function phenotypes, with respect to FXS protein FMRP. We hypothesize *YTHDF2* loss-of-function would lead to microcephaly due to increased FMRP binding and lack of m^6-mRNA degradation, extended cell cycle progression, and reduced neurogenesis. As the gene is highly conserved and knockout models are embryonic lethal, likely loss-of-function mutations in humans lead to disease pathogenicity or are incompatible with life. Inversely, *YTHDF2* duplication would lead to megalencephaly following increased m^6A-mRNA degradation as YTHDF2 outcompetes FMRP, neural progenitor cell (NPC) overabundance, and increased neurogenesis.

Expanding beyond *YTHDF2*, we identified an additional *de novo* LGD variant in an SSC ASD-M proband impacting another YTH-domain-containing m^6A-RNA reader, *YTHDC1*. The encoded protein promotes recruitment of splicing factors and facilitates nuclear export of modified transcripts [139]. Where gain of *YTHDF2* may lead to a decrease in overall m^6A-mRNA by promoting transcript degradation, conversely the loss of *YTHDC1* would likely result in a depletion of spliced and cytoplasmic transcripts [140]. Interestingly, FMRP also facilitates nuclear export of m^6A-labeled RNAs prevalent during neural differentiation [132,141,142]. While m^6A-RNA regulation genes were not significantly enriched in our identified ASD-DM candidate genes, none were observed in SSC ASD-N or in TD siblings [143], suggesting that additional genes within this pathway may contribute to ASD-DM. Indeed, FMRP has been shown to repress translation of m^6A RNAs, through competition for binding and inhibition of m^6A reader *YTHDF1* [144]. These ties between m^6A mRNA readers and FMRP suggest a fine balance of select transcripts, in which up- or down-regulation may impact early neurodevelopment and autistic phenotypes. Further, the m^6A-labeled mRNA flavivirus ZIKA is associated with severe congenital microcephaly, with *YTHDF2* found to bind and destabilize viral RNA [145,146]. These antiviral functions are controlled in part by the *METTL3* methyltransferase, which labels viral RNA for degradation, and whose knockout models are also associated with a reduced brain size in mice [147]. Together the m^6A-mRNA pathway—including YTH-domain proteins and m^6A de/methyltransferases — represents a compelling future area of study in regard to ASD and brain-size phenotypes.

Though new insights were achieved from our study, we would like to highlight some limitations. Due to the dearth of MRI evidence, not all SSC ASD-M probands included in this study will meet the criteria for

ASD-DM. We do expect the overlap to be significant, as macrocephaly has previously been found to be highly correlated with megalencephaly, with an increased correlation in young children [148]. This is supported by the majority of APP ASD-DM probands also meeting the criteria for macrocephaly (82%), Additionally, zebrafish, with a forebrain that most closely resembles the mammalian neocortex [149], may not be a suitable model for all ASD-DM candidate genes. This is highlighted by our microcephaly finding in *ryr3* knockout zebrafish larvae, counter to the APP proband phenotype. Further, our study did not identify any measurable morphometric differences in *chd8* crispants versus controls at 3 dpf (Figure 3), counter to previous studies showing megalencephaly in crispants, morpholino knockdown, and stable KO lines at young larval stages [36,96]. We do note that inconsistencies exist across published *CHD8* KO models, with a recent stable line reported to show decreased brain size at 6 dpf [35]. Nevertheless, characterizing genes implicated in ASD and other neurodevelopmental conditions in zebrafish has been successfully demonstrated across hundreds of genes (reviewed by [150–154]).

Overall, this study represents a significant increase in the number ASD-DM and ASD-M proband genomes analyzed in search of candidate genes. The 153 candidate ASD-DM genes introduced here greatly expand our knowledge of the genetic factors specifically contributing to this severe subphenotype of ASD. With this expanded list of ASD-DM candidate genes, network analysis can now be leveraged to identify additional candidate genes with similar gene functions to known ASD-DM genes. Our study introduces two novel ASD-DM candidate genes connected with head-size phenotypes in a zebrafish model system and 141 novel unvalidated ASD-DM candidate genes (Table 1). Finally, our research establishes a roadmap for the rapid functional characterization of these putative risk genes, demonstrating the methodology needed to validate these candidates going forward.

FIGURE LEGENDS

Figure 1. Macrocephaly level of candidate ASD-DM and ASD-M genes. (A) A histogram representing the number of SSC probands v. head circumference percentiles shows a skew towards larger head-sizes compared to age and sex-matched typically developing children. The red bar designates those meeting the criteria for macrocephaly. The dashed line represents the distribution mean. **(B)** ASD-DM and ASD-M genes listed by their identified proband's head circumference percentiles show genes previously associated with ASD-DM (first gray quadrant) are more likely to be associated with a higher head circumference percentiles than genes previously associated with autism (second white quadrant) and DM (third gray quadrant) alone. Color represents the macrocephaly type. DM, disproportionate macrocephaly; RM, relative macrocephaly; SO, somatic overgrowth.

Figure 2. Network analysis and gene ontology of ASD-DM candidate genes. ASD-DM candidate genes from SSC (teal), APP (purple), and Wu (navy) probands are connected in a network via active interactions as determined by STRING [50]. Background colors represent shared GO molecular functions. Disconnected gene nodes are not included.

Figure 3. **Zebrafish CRISPR knockout embryos for the rapid validation of ASD-DM genes.** Phenotyping knockout zebrafish morphometric measurements using the VAST BioImaging System, we identified *ryr3* and *ythdf2* as having reduced head size compared to a negative scrambled control. Seizure-

like activity in the presence of PTZ was assessed using ZebraBox video motion tracking. Circle size represents the inverse Wilcoxon T-test p-value. Circle color represents the fold change compared to a negative scrambled control.

Figure 4. Disrupting *ythdf2* in zebrafish is associated with head and brain size phenotypes. (**A**) Copy-number-estimate plot (QuickMer2) using sequencing data from the APP proband harboring a *de novo* duplication a 109-kb duplication on chromosome 1 compared to their parents harboring two diploid copies. (**B**) IGV plot showing discordant reads in the APP proband supporting a tandem duplication. (**C**) An illustration of the tandem duplication on chromosome 1 in an APP proband encompassing *GMEB1* and all but the last exon of *YTHDF2*. (**D**) Head size of mRNA injected zebrafish, estimated via telencephalon measurement, are significantly increased after *YTHDF2* mRNA microinjection into zebrafish embryos (Wilcoxon T-test p-value = 0.0013), and unchanged in *GMEB1* mRNA injected embryos at 3 dpf (Wilcoxon T-test p-value = 0.8). (**E**) Knockout and mRNA injected zebrafish harboring a pan neuronal marker reveal brain size differences at 3 dpf. Knockout embryos show significantly decreased midbrain volume (Wilcoxon T-test, p-value = 0.003). mRNA injected embryos show both significantly increased midbrain (Wilcoxon T-test, p-value = 0.007) and forebrain (Wilcoxon T-test, p-value = 0.0005). (**F**) Representative control, knockout, and mRNA injected zebrafish images from wildtype embryos imaged with the VAST bioimaging system and HuC embryos harboring a pan neuronal fluorescent marker. Scale bar is 100 μm. (**G**) Hierarchical clustering of 19,141 cells across all conditions into 9 broad cell types based on the expression of gene markers. Joint kernel density estimation was calculated from all 15 FMRP-target DEGs (Nebulosa) highlighting higher expression within a sub-type of brain cells. (**H**) Volcano plots showing DEGs across all cell-types within *ythdf2* knockout (top left) and *YTHDF2* mRNA overexpression (bottom left) conditions relative to controls. DEGs with absolute $\log_2$`FC ≥ 1 and p-adj ≤ 0.05 are colored (upregulated as red, downregulated as blue). Average` $\log_2$FC across all expressed genes shows no significant difference between knockout and overexpression groups (top right), while average $\log_2$FC across orthologs of all 675 FMRP-target genes expressed in both groups shows a reduction in overexpression relative to knockout. (**I**) Hierarchical sub-clustering of 12,066 brain cells across all conditions into 18 cell types based on the expression of gene markers. Joint kernel density estimation plot highlights higher FMRP-target DEGs expression within forebrain and mid- and hindbrain neurons. Average $\log_2$FC for all 15 genes across knockout and overexpression with respect to controls is shown. All *p*-values in this figure are represented as: <0.05*, <0.01**, <0.001***.

Figure 5. A potential role for *YTHDF2* in ASD-DM. Proposed model of *YTHDF2* loss- or gain-of-function phenotypes, with respect to FXS protein FMRP. We hypothesize *YTHDF2* loss-of-function would lead to microcephaly due to increased FMRP binding and lack of m6-mRNA degradation, extended cell cycle progression, and reduced neurogenesis. As the gene is highly conserved and knockout models are embryonic lethal, likely loss-of-function mutations in humans lead to disease pathogenicity or are incompatible with life. Inversely, *YTHDF2* duplication would lead to megalencephaly following increased m^6A-mRNA degradation as YTHDF2 outcompetes FMRP, neural progenitor cell (NPC) overabundance, and increased neurogenesis.

REFERENCES

1. Maenner MJ. Prevalence and Characteristics of Autism Spectrum Disorder Among Children Aged 8 Years — Autism and Developmental Disabilities Monitoring Network, 11 Sites, United States, 2020. MMWR Surveill Summ [Internet]. 2023 [cited 2024 Aug 5];72. Available from: https://www.cdc.gov/mmwr/volumes/72/ss/ss7202a1.htm

2. Sandin S, Lichtenstein P, Kuja-Halkola R, Larsson H, Hultman CM, Reichenberg A. The familial risk of autism. JAMA. 2014;311:1770–7.

3. Sandin S, Schendel D, Magnusson P, Hultman C, Surén P, Susser E, et al. Autism risk associated with parental age and with increasing difference in age between the parents. Mol Psychiatry. 2016;21:693–700.

4. Castelbaum L, Sylvester CM, Zhang Y, Yu Q, Constantino JN. On the Nature of Monozygotic Twin Concordance and Discordance for Autistic Trait Severity: A Quantitative Analysis. Behav Genet. 2020;50:263–72.

5. Satterstrom FK, Kosmicki JA, Wang J, Breen MS, De Rubeis S, An J-Y, et al. Large-Scale Exome Sequencing Study Implicates Both Developmental and Functional Changes in the Neurobiology of Autism. Cell. 2020;180:568–84.e23.

6. Fu JM, Satterstrom FK, Peng M, Brand H, Collins RL, Dong S, et al. Rare coding variation provides insight into the genetic architecture and phenotypic context of autism. Nat Genet. 2022;54:1320–31.

7. Leblond CS, Le T-L, Malesys S, Cliquet F, Tabet A-C, Delorme R, et al. Operative list of genes associated with autism and neurodevelopmental disorders based on database review. Mol Cell Neurosci. 2021;113:103623.

8. Fischbach GD, Lord C. The Simons Simplex Collection: a resource for identification of autism genetic risk factors. Neuron. 2010;68:192–5.

9. Iossifov I, O'Roak BJ, Sanders SJ, Ronemus M, Krumm N, Levy D, et al. The contribution of de novo coding mutations to autism spectrum disorder. Nature. 2014;515:216–21.

10. Sanders SJ, Murtha MT, Gupta AR, Murdoch JD, Raubeson MJ, Willsey AJ, et al. De novo mutations revealed by whole-exome sequencing are strongly associated with autism. Nature. 2012;485:237–41.

11. Belyeu JR, Brand H, Wang H, Zhao X, Pedersen BS, Feusier J, et al. De novo structural mutation rates and gamete-of-origin biases revealed through genome sequencing of 2,396 families. Am J Hum Genet. 2021;108:597–607.

12. An J-Y, Lin K, Zhu L, Werling DM, Dong S, Brand H, et al. Genome-wide de novo risk score implicates promoter variation in autism spectrum disorder. Science. 2018;362:eaat6576.

13. Zhou J, Park CY, Theesfeld CL, Wong AK, Yuan Y, Scheckel C, et al. Whole-genome deep-learning analysis identifies contribution of noncoding mutations to autism risk. Nat Genet. 2019;51:973–80.

14. Antaki D, Guevara J, Maihofer AX, Klein M, Gujral M, Grove J, et al. A phenotypic spectrum of autism is attributable to the combined effects of rare variants, polygenic risk and sex. Nat Genet. 2022;1–9.

15. Warrier V, Zhang X, Reed P, Havdahl A, Moore TM, Cliquet F, et al. Genetic correlates of

phenotypic heterogeneity in autism [Internet]. Available from: http://dx.doi.org/10.1101/2020.07.21.20159228

16. Zhou X, Feliciano P, Shu C, Wang T, Astrovskaya I, Hall JB, et al. Integrating de novo and inherited variants in 42,607 autism cases identifies mutations in new moderate-risk genes. Nat Genet. 2022;54:1305–19.

17. Trost B, Thiruvahindrapuram B, Chan AJS, Engchuan W, Higginbotham EJ, Howe JL, et al. Genomic architecture of autism from comprehensive whole-genome sequence annotation. Cell. 2022;185:4409–27.e18.

18. Rylaarsdam L, Guemez-Gamboa A. Genetic Causes and Modifiers of Autism Spectrum Disorder. Front Cell Neurosci. 2019;13:385.

19. Wang T, Kim CN, Bakken TE, Gillentine MA, Henning B, Mao Y, et al. Integrated gene analyses of de novo variants from 46,612 trios with autism and developmental disorders. Proc Natl Acad Sci U S A. 2022;119:e2203491119.

20. Rolland T, Cliquet F, Anney RJL, Moreau C, Traut N, Mathieu A, et al. Phenotypic effects of genetic variants associated with autism. Nat Med. 2023;29:1671–80.

21. Wilfert AB, Turner TN, Murali SC, Hsieh P, Sulovari A, Wang T, et al. Recent ultra-rare inherited variants implicate new autism candidate risk genes. Nat Genet. 2021;53:1125–34.

22. Cirnigliaro M, Chang TS, Arteaga SA, Pérez-Cano L, Ruzzo EK, Gordon A, et al. The contributions of rare inherited and polygenic risk to ASD in multiplex families. Proc Natl Acad Sci U S A. 2023;120:e2215632120.

23. Liu X-Q, Paterson AD, Szatmari P, Autism Genome Project Consortium. Genome-wide linkage analyses of quantitative and categorical autism subphenotypes. Biol Psychiatry. 2008;64:561–70.

24. Amaral DG, Li D, Libero L, Solomon M, Van de Water J, Mastergeorge A, et al. In pursuit of neurophenotypes: The consequences of having autism and a big brain [Internet]. Autism Research. 2017. p. 711–22. Available from: http://dx.doi.org/10.1002/aur.1755

25. Chawarska K. Early Generalized Overgrowth in Boys With Autism [Internet]. Archives of General Psychiatry. 2011. p. 1021. Available from: http://dx.doi.org/10.1001/archgenpsychiatry.2011.106

26. Nordahl CW, Lange N, Li DD, Barnett LA, Lee A, Buonocore MH, et al. Brain enlargement is associated with regression in preschool-age boys with autism spectrum disorders. Proc Natl Acad Sci U S A. 2011;108:20195–200.

27. Sacco R, Militerni R, Frolli A, Bravaccio C, Gritti A, Elia M, et al. Clinical, morphological, and biochemical correlates of head circumference in autism. Biol Psychiatry. 2007;62:1038–47.

28. Hormozdiari F, Penn O, Borenstein E, Eichler EE. The discovery of integrated gene networks for autism and related disorders. Genome Res. 2015;25:142–54.

29. Krishnan A, Zhang R, Yao V, Theesfeld CL, Wong AK, Tadych A, et al. Genome-wide characterization of genetic and functional dysregulation in autism spectrum disorder [Internet]. bioRxiv. bioRxiv; 2016. Available from: http://dx.doi.org/10.1101/057828

30. O'Roak BJ, Vives L, Fu W, Egertson JD, Stanaway IB, Phelps IG, et al. Multiplex targeted

sequencing identifies recurrently mutated genes in autism spectrum disorders. Science. 2012;338:1619–22.

31. Willsey AJ, Sanders SJ, Li M, Dong S, Tebbenkamp AT, Muhle RA, et al. Coexpression networks implicate human midfetal deep cortical projection neurons in the pathogenesis of autism. Cell. 2013;155:997–1007.

32. Wu H, Li H, Bai T, Han L, Ou J, Xun G, et al. Phenotype-to-genotype approach reveals head-circumference-associated genes in an autism spectrum disorder cohort. Clin Genet. 2020;97:338–46.

33. Abreu MS de, de Abreu MS, Genario R, Giacomini ACV, Demin KA, Lakstygal AM, et al. Zebrafish as a Model of Neurodevelopmental Disorders [Internet]. Neuroscience. 2020. p. 3–11. Available from: http://dx.doi.org/10.1016/j.neuroscience.2019.08.034

34. Howe K, Clark MD, Torroja CF, Torrance J, Berthelot C, Muffato M, et al. The zebrafish reference genome sequence and its relationship to the human genome. Nature. 2013;496:498–503.

35. Weinschutz Mendes H, Neelakantan U, Liu Y, Fitzpatrick SE, Chen T, Wu W, et al. High-throughput functional analysis of autism genes in zebrafish identifies convergence in dopaminergic and neuroimmune pathways. Cell Rep. 2023;42:112243.

36. Bernier R, Golzio C, Xiong B, Stessman HA, Coe BP, Penn O, et al. Disruptive CHD8 mutations define a subtype of autism early in development. Cell. 2014;158:263–76.

37. Thyme SB, Pieper LM, Li EH, Pandey S, Wang Y, Morris NS, et al. Phenotypic Landscape of Schizophrenia-Associated Genes Defines Candidates and Their Shared Functions. Cell. 2019;177:478–91.e20.

38. Golzio C, Willer J, Talkowski ME, Oh EC, Taniguchi Y, Jacquemont S, et al. KCTD13 is a major driver of mirrored neuroanatomical phenotypes of the 16p11.2 copy number variant. Nature. 2012;485:363–7.

39. Pulak R. Tools for automating the imaging of zebrafish larvae. Methods. 2016;96:118–26.

40. Colón-Rodríguez A, Uribe-Salazar JM, Weyenberg KB, Sriram A, Quezada A, Kaya G, et al. Assessment of autism zebrafish mutant models using a high-throughput larval phenotyping platform. Front Cell Dev Biol. 2020;8:586296.

41. Lee JK, Andrews DS, Ozonoff S, Solomon M, Rogers S, Amaral DG, et al. Longitudinal Evaluation of Cerebral Growth Across Childhood in Boys and Girls With Autism Spectrum Disorder. Biol Psychiatry. 2021;90:286–94.

42. Chan AJS, Engchuan W, Reuter MS, Wang Z, Thiruvahindrapuram B, Trost B, et al. Genome-wide rare variant score associates with morphological subtypes of autism spectrum disorder. Nat Commun. 2022;13:6463.

43. C Yuen RK, Merico D, Bookman M, L Howe J, Thiruvahindrapuram B, Patel RV, et al. Whole genome sequencing resource identifies 18 new candidate genes for autism spectrum disorder. Nat Neurosci. 2017;20:602–11.

44. Klein S, Sharifi-Hannauer P, Martinez-Agosto JA. Macrocephaly as a clinical indicator of genetic subtypes in autism. Autism Res. 2013;6:51–6.

45. Rollins JD, Collins JS, Holden KR. United States head circumference growth reference charts: birth to 21 years. J Pediatr. 2010;156:907–13.e2.

46. Centers for Disease Control and Prevention, National Center for Health Statistics. Data Table of Stature-for-age Charts [Internet]. Centers for Disease Control and Prevention (CDC). 2001 [cited 2022 Nov 26]. Available from: https://www.cdc.gov/growthcharts/html_charts/statage.htm#males

47. Sherry ST, Ward MH, Kholodov M, Baker J, Phan L, Smigielski EM, et al. dbSNP: the NCBI database of genetic variation. Nucleic Acids Res. 2001;29:308–11.

48. 1000 Genomes Project Consortium, Auton A, Brooks LD, Durbin RM, Garrison EP, Kang HM, et al. A global reference for human genetic variation. Nature. 2015;526:68–74.

49. Thorvaldsdóttir H, Robinson JT, Mesirov JP. Integrative Genomics Viewer (IGV): high-performance genomics data visualization and exploration. Brief Bioinform. 2013;14:178–92.

50. Szklarczyk D, Franceschini A, Wyder S, Forslund K, Heller D, Huerta-Cepas J, et al. STRING v10: protein-protein interaction networks, integrated over the tree of life. Nucleic Acids Res. 2015;43:D447–52.

51. Shannon P, Markiel A, Ozier O, Baliga NS, Wang JT, Ramage D, et al. Cytoscape: a software environment for integrated models of biomolecular interaction networks. Genome Res. 2003;13:2498–504.

52. Sherman BT, Hao M, Qiu J, Jiao X, Baseler MW, Lane HC, et al. DAVID: a web server for functional enrichment analysis and functional annotation of gene lists (2021 update). Nucleic Acids Res. 2022;50:W216–21.

53. Moreno-Mateos MA, Vejnar CE, Beaudoin J-D, Fernandez JP, Mis EK, Khokha MK, et al. CRISPRscan: designing highly efficient sgRNAs for CRISPR-Cas9 targeting in vivo. Nat Methods. 2015;12:982–8.

54. Wu RS, Lam II, Clay H, Duong DN, Deo RC, Coughlin SR. A rapid method for directed gene knockout for screening in G0 zebrafish. Dev Cell. 2018;46:112–25.e4.

55. Jao L-E, Wente SR, Chen W. Efficient multiplex biallelic zebrafish genome editing using a CRISPR nuclease system. Proc Natl Acad Sci U S A. 2013;110:13904–9.

56. Lindsay H, Burger A, Biyong B, Felker A, Hess C, Zaugg J, et al. CrispRVariants charts the mutation spectrum of genome engineering experiments. Nat Biotechnol. 2016;34:701–2.

57. The Status, Quality, and Expansion of the NIH Full-Length cDNA Project: The Mammalian Gene Collection (MGC) [Internet]. Genome Research. 2004. p. 2121–7. Available from: http://dx.doi.org/10.1101/gr.2596504

58. Yuan S, Sun Z. Microinjection of mRNA and morpholino antisense oligonucleotides in zebrafish embryos. J Vis Exp [Internet]. 2009; Available from: http://dx.doi.org/10.3791/1113

59. Teixidó E, Kießling TR, Krupp E, Quevedo C, Muriana A, Scholz S. Automated morphological feature assessment for zebrafish embryo developmental toxicity screens. Toxicol Sci. 2019;167:438–49.

60. Ahlmann-Eltze C, Patil I. ggsignif: R Package for Displaying Significance Brackets for “ggplot2” [Internet]. Available from: http://dx.doi.org/10.31234/osf.io/7awm6

61. Lee DA, Oikonomou G, Prober DA. Large-scale Analysis of Sleep in Zebrafish. Bio Protoc. 2022;12:e4313.

62. Griffin A, Carpenter C, Liu J, Paterno R, Grone B, Hamling K, et al. Phenotypic analysis of catastrophic childhood epilepsy genes. Commun Biol. 2021;4:680.

63. Cao J, Shendure J. sci-RNA-seq3. 2020 [cited 2024 Aug 13]; Available from: https://www.protocols.io/view/sci-rna-seq3-36wgq578ogk5/v1

64. Lawson ND, Li R, Shin M, Grosse A, Yukselen O, Stone OA, et al. An improved zebrafish transcriptome annotation for sensitive and comprehensive detection of cell type-specific genes. Elife [Internet]. 2020;9. Available from: http://dx.doi.org/10.7554/eLife.55792

65. Hao Y, Hao S, Andersen-Nissen E, Mauck WM 3rd, Zheng S, Butler A, et al. Integrated analysis of multimodal single-cell data. Cell. 2021;184:3573–87.e29.

66. McGinnis CS, Murrow LM, Gartner ZJ. DoubletFinder: Doublet Detection in Single-Cell RNA Sequencing Data Using Artificial Nearest Neighbors. Cell Syst. 2019;8:329–37.e4.

67. Zhang H, Wang H, Shen X, Jia X, Yu S, Qiu X, et al. The landscape of regulatory genes in brain-wide neuronal phenotypes of a vertebrate brain. Elife [Internet]. 2021;10. Available from: http://dx.doi.org/10.7554/eLife.68224

68. Raj B, Farrell JA, Liu J, El Kholtei J, Carte AN, Navajas Acedo J, et al. Emergence of Neuronal Diversity during Vertebrate Brain Development. Neuron. 2020;108:1058–74.e6.

69. Bradford YM, Van Slyke CE, Ruzicka L, Singer A, Eagle A, Fashena D, et al. Zebrafish information network, the knowledgebase for Danio rerio research. Genetics [Internet]. 2022;220. Available from: http://dx.doi.org/10.1093/genetics/iyac016

70. Darnell JC, Van Driesche SJ, Zhang C, Hung KYS, Mele A, Fraser CE, et al. FMRP stalls ribosomal translocation on mRNAs linked to synaptic function and autism. Cell. 2011;146:247–61.

71. Kolberg L, Raudvere U, Kuzmin I, Adler P, Vilo J, Peterson H. g:Profiler—interoperable web service for functional enrichment analysis and gene identifier mapping (2023 update). Nucleic Acids Res. 2023;51:W207–12.

72. Marsh SE. scCustomize: custom visualizations & functions for streamlined analyses of single cell sequencing. Preprint at https://doi org/105281/zenodo.

73. Bunis DG, Andrews J, Fragiadakis GK, Burt TD, Sirota M. dittoSeq: universal user-friendly single-cell and bulk RNA sequencing visualization toolkit. Bioinformatics. 2021;36:5535–6.

74. Trdy S. Nebulosa. Novum Publishing; 2011.

75. Nordahl CW, Andrews DS, Dwyer P, Waizbard-Bartov E, Restrepo B, Lee JK, et al. The Autism Phenome Project: Toward Identifying Clinically Meaningful Subgroups of Autism. Front Neurosci. 2021;15:786220.

76. Ohta H, Nordahl CW, Iosif A-M, Lee A, Rogers S, Amaral DG. Increased Surface Area, but not Cortical Thickness, in a Subset of Young Boys With Autism Spectrum Disorder. Autism Res. 2016;9:232–48.

77. Brunetti-Pierri N, Berg JS, Scaglia F, Belmont J, Bacino CA, Sahoo T, et al. Recurrent reciprocal 1q21.1 deletions and duplications associated with microcephaly or macrocephaly and developmental and behavioral abnormalities. Nat Genet. 2008;40:1466–71.

78. Dolcetti A, Silversides CK, Marshall CR, Lionel AC, Stavropoulos DJ, Scherer SW, et al. 1q21.1 Microduplication expression in adults. Genet Med. 2013;15:282–9.

79. Sherry ST, Ward M, Sirotkin K. dbSNP-database for single nucleotide polymorphisms and other classes of minor genetic variation. Genome Res. 1999;9:677–9.

80. Abrahams BS, Arking DE, Campbell DB, Mefford HC, Morrow EM, Weiss LA, et al. SFARI Gene 2.0: a community-driven knowledgebase for the autism spectrum disorders (ASDs). Mol Autism. 2013;4:36.

81. Karczewski KJ, Francioli LC, Tiao G, Cummings BB, Alföldi J, Wang Q, et al. The mutational constraint spectrum quantified from variation in 141,456 humans. Nature. 2020;581:434–43.

82. Samocha KE, Kosmicki JA, Karczewski KJ, O'Donnell-Luria AH, Pierce-Hoffman E, MacArthur DG, et al. Regional missense constraint improves variant deleteriousness prediction [Internet]. bioRxiv. bioRxiv; 2017. Available from: http://dx.doi.org/10.1101/148353

83. Koire A, Katsonis P, Kim YW, Buchovecky C, Wilson SJ, Lichtarge O. A method to delineate de novo missense variants across pathways prioritizes genes linked to autism. Sci Transl Med [Internet]. 2021;13. Available from: http://dx.doi.org/10.1126/scitranslmed.abc1739

84. Lasalle JM. Autism genes keep turning up chromatin. OA Autism. 2013;1:14.

85. Hoffmann A, Spengler D. Single-Cell Transcriptomics Supports a Role of CHD8 in Autism [Internet]. International Journal of Molecular Sciences. 2021. p. 3261. Available from: http://dx.doi.org/10.3390/ijms22063261

86. Pinto D, Delaby E, Merico D, Barbosa M, Merikangas A, Klei L, et al. Convergence of genes and cellular pathways dysregulated in autism spectrum disorders. Am J Hum Genet. 2014;94:677–94.

87. Brooks-Kayal A. Epilepsy and autism spectrum disorders: are there common developmental mechanisms? Brain Dev. 2010;32:731–8.

88. Pirozzi F, Nelson B, Mirzaa G. From microcephaly to megalencephaly: determinants of brain size. Dialogues Clin Neurosci. 2018;20:267–82.

89. Reijnders MRF, Kousi M, van Woerden GM, Klein M, Bralten J, Mancini GMS, et al. Variation in a range of mTOR-related genes associates with intracranial volume and intellectual disability [Internet]. Nature Communications. 2017. Available from: http://dx.doi.org/10.1038/s41467-017-00933-6

90. Yeung KS, Tso WWY, Ip JJK, Mak CCY, Leung GKC, Tsang MHY, et al. Identification of mutations in the PI3K-AKT-mTOR signalling pathway in patients with macrocephaly and developmental delay and/or autism [Internet]. Molecular Autism. 2017. Available from: http://dx.doi.org/10.1186/s13229-017-0182-4

91. Kozol RA, Abrams AJ, James DM, Buglo E, Yan Q, Dallman JE. Function Over Form: Modeling Groups of Inherited Neurological Conditions in Zebrafish. Front Mol Neurosci. 2016;9:55.

92. Kroll F, Powell GT, Ghosh M, Gestri G, Antinucci P, Hearn TJ, et al. A simple and effective F0

knockout method for rapid screening of behaviour and other complex phenotypes. Elife [Internet]. 2021;10. Available from: http://dx.doi.org/10.7554/eLife.59683

93. Nilipour Y, Nafissi S, Varasteh V, Hossein-Nejad H, Tonekaboni S, Ravenscroft G, et al. Ryanodine receptor type 3 (RYR3) as a novel gene associated with nemaline myopathy and fibre type disproportion [Internet]. Neuromuscular Disorders. 2016. p. S137. Available from: http://dx.doi.org/10.1016/j.nmd.2016.06.188

94. Sokpor G, Xie Y, Nguyen HP, Tuoc T. Emerging Role of m A Methylome in Brain Development: Implications for Neurological Disorders and Potential Treatment. Front Cell Dev Biol. 2021;9:656849.

95. Zhao BS, Wang X, Beadell AV, Lu Z, Shi H, Kuuspalu A, et al. mA-dependent maternal mRNA clearance facilitates zebrafish maternal-to-zygotic transition. Nature. 2017;542:475–8.

96. Sugathan A, Biagioli M, Golzio C, Erdin S, Blumenthal I, Manavalan P, et al. *CHD8* regulates neurodevelopmental pathways associated with autism spectrum disorder in neural progenitors. Proc Natl Acad Sci U S A. 2014;111:E4468–77.

97. Frye R. A review of traditional and novel treatments for seizures in autism spectrum disorder: findings from a systematic review and expert panel [Internet]. Frontiers in Public Health. 2013. Available from: http://dx.doi.org/10.3389/fpubh.2013.00031

98. Frye RE, Casanova MF, Fatemi SH, Folsom TD, Reutiman TJ, Brown GL, et al. Neuropathological Mechanisms of Seizures in Autism Spectrum Disorder. Front Neurosci. 2016;10:192.

99. Baraban SC, Taylor MR, Castro PA, Baier H. Pentylenetetrazole induced changes in zebrafish behavior, neural activity and c-fos expression. Neuroscience. 2005;131:759–68.

100. Nevado J, Mergener R, Palomares-Bralo M, Souza KR, Vallespín E, Mena R, et al. New microdeletion and microduplication syndromes: A comprehensive review. Genet Mol Biol. 2014;37:210–9.

101. Fromme JC, Munson M. Capturing endosomal vesicles at the Golgi. Nat Cell Biol. 2017;19:1384–6.

102. Salmela E, Renvall H, Kujala J, Hakosalo O, Illman M, Vihla M, et al. Evidence for genetic regulation of the human parieto-occipital 10-Hz rhythmic activity. Eur J Neurosci. 2016;44:1963–71.

103. Shen F, Kidd JM. Rapid, Paralog-Sensitive CNV Analysis of 2457 Human Genomes Using QuicK-mer2. Genes [Internet]. 2020;11. Available from: http://dx.doi.org/10.3390/genes11020141

104. Stamova BS, Tian Y, Nordahl CW, Shen MD, Rogers S, Amaral DG, et al. Evidence for differential alternative splicing in blood of young boys with autism spectrum disorders. Mol Autism. 2013;4:30.

105. Nakagawa T, Tsuruma K, Uehara T, Nomura Y. GMEB1, a novel endogenous caspase inhibitor, prevents hypoxia- and oxidative stress-induced neuronal apoptosis. Neurosci Lett. 2008;438:34–7.

106. Singh T, Poterba T, Curtis D, Akil H, Al Eissa M, Barchas JD, et al. Rare coding variants in ten genes confer substantial risk for schizophrenia. Nature. 2022;604:509–16.

107. Park HC, Kim CH, Bae YK, Yeo SY, Kim SH, Hong SK, et al. Analysis of upstream elements in the HuC promoter leads to the establishment of transgenic zebrafish with fluorescent neurons. Dev Biol. 2000;227:279–93.

108. Cao J, Spielmann M, Qiu X, Huang X, Ibrahim DM, Hill AJ, et al. The single-cell transcriptional landscape of mammalian organogenesis. Nature. 2019;566:496–502.

109. GTEx Consortium. The GTEx Consortium atlas of genetic regulatory effects across human tissues. Science. 2020;369:1318–30.

110. Kontur C, Jeong M, Cifuentes D, Giraldez AJ. Ythdf mA Readers Function Redundantly during Zebrafish Development. Cell Rep. 2020;33:108598.

111. Yang H, Luan Y, Liu T, Lee HJ, Fang L, Wang Y, et al. A map of cis-regulatory elements and 3D genome structures in zebrafish. Nature. 2020;588:337–43.

112. White RJ, Collins JE, Sealy IM, Wali N, Dooley CM, Digby Z, et al. A high-resolution mRNA expression time course of embryonic development in zebrafish [Internet]. Available from: http://dx.doi.org/10.1101/107631

113. Shu H, Donnard E, Liu B, Jung S, Wang R, Richter JD. FMRP links optimal codons to mRNA stability in neurons. Proc Natl Acad Sci U S A. 2020;117:30400–11.

114. Weissberg O, Elliott E. The Mechanisms of CHD8 in Neurodevelopment and Autism Spectrum Disorders. Genes [Internet]. 2021;12. Available from: http://dx.doi.org/10.3390/genes12081133

115. Moyses-Oliveira M, Yadav R, Erdin S, Talkowski ME. New gene discoveries highlight functional convergence in autism and related neurodevelopmental disorders. Curr Opin Genet Dev. 2020;65:195–206.

116. Stolerman ES, Francisco E, Stallworth JL, Jones JR, Monaghan KG, Keller-Ramey J, et al. Genetic variants in the KDM6B gene are associated with neurodevelopmental delays and dysmorphic features. Am J Med Genet A. 2019;179:1276–86.

117. Fregeau B, Kim BJ, Hernández-García A, Jordan VK, Cho MT, Schnur RE, et al. De Novo Mutations of RERE Cause a Genetic Syndrome with Features that Overlap Those Associated with Proximal 1p36 Deletions. Am J Hum Genet. 2016;98:963–70.

118. Le Duc D, Giulivi C, Hiatt SM, Napoli E, Panoutsopoulos A, Harlan De Crescenzo A, et al. Pathogenic WDFY3 variants cause neurodevelopmental disorders and opposing effects on brain size. Brain. 2019;142:2617–30.

119. Coit P, Ortiz-Fernandez L, Lewis EE, McCune WJ, Maksimowicz-McKinnon K, Sawalha AH. A longitudinal and transancestral analysis of DNA methylation patterns and disease activity in lupus patients. JCI Insight [Internet]. 2020;5. Available from: http://dx.doi.org/10.1172/jci.insight.143654

120. Doamekpor SK, Lee J-W, Hepowit NL, Wu C, Charenton C, Leonard M, et al. Structure and function of the yeast listerin (Ltn1) conserved N-terminal domain in binding to stalled 60S ribosomal subunits. Proc Natl Acad Sci U S A. 2016;113:E4151–60.

121. Li M, Zhao X, Wang W, Shi H, Pan Q, Lu Z, et al. Ythdf2-mediated mA mRNA clearance modulates neural development in mice. Genome Biol. 2018;19:69.

122. Li Z, Qian P, Shao W, Shi H, He XC, Gogol M, et al. Suppression of mA reader Ythdf2 promotes hematopoietic stem cell expansion. Cell Res. 2018;28:904–17.

123. Wang X, Lu Z, Gomez A, Hon GC, Yue Y, Han D, et al. N6-methyladenosine-dependent regulation

of messenger RNA stability. Nature. 2014;505:117–20.

124. Du H, Zhao Y, He J, Zhang Y, Xi H, Liu M, et al. YTHDF2 destabilizes m(6)A-containing RNA through direct recruitment of the CCR4-NOT deadenylase complex. Nat Commun. 2016;7:12626.

125. Heck AM, Russo J, Wilusz J, Nishimura EO, Wilusz CJ. YTHDF2 destabilizes mA-modified neural-specific RNAs to restrain differentiation in induced pluripotent stem cells. RNA. 2020;26:739–55.

126. Fei Q, Zou Z, Roundtree IA, Sun H-L, He C. YTHDF2 promotes mitotic entry and is regulated by cell cycle mediators. PLoS Biol. 2020;18:e3000664.

127. Wu R, Liu Y, Zhao Y, Bi Z, Yao Y, Liu Q, et al. mA methylation controls pluripotency of porcine induced pluripotent stem cells by targeting SOCS3/JAK2/STAT3 pathway in a YTHDF1/YTHDF2-orchestrated manner. Cell Death Dis. 2019;10:171.

128. Kaufmann WE, Kidd SA, Andrews HF, Budimirovic DB, Esler A, Haas-Givler B, et al. Autism Spectrum Disorder in Fragile X Syndrome: Cooccurring Conditions and Current Treatment. Pediatrics. 2017;139:S194–206.

129. Sacco R, Gabriele S, Persico AM. Head circumference and brain size in autism spectrum disorder: A systematic review and meta-analysis. Psychiatry Res. 2015;234:239–51.

130. Hazlett HC, Poe MD, Lightbody AA, Styner M, MacFall JR, Reiss AL, et al. Trajectories of early brain volume development in fragile X syndrome and autism. J Am Acad Child Adolesc Psychiatry. 2012;51:921–33.

131. Zhang F, Kang Y, Wang M, Li Y, Xu T, Yang W, et al. Fragile X mental retardation protein modulates the stability of its m6A-marked messenger RNA targets. Hum Mol Genet. 2018;27:3936–50.

132. Hsu PJ, Shi H, Zhu AC, Lu Z, Miller N, Edens BM, et al. The RNA-binding protein FMRP facilitates the nuclear export of -methyladenosine-containing mRNAs. J Biol Chem. 2019;294:19889–95.

133. Zhang G, Xu Y, Wang X, Zhu Y, Wang L, Zhang W, et al. Dynamic FMR1 granule phase switch instructed by m6A modification contributes to maternal RNA decay. Nat Commun. 2022;13:859.

134. Plioplys AV, Hemmens SE, Regan CM. Expression of a neural cell adhesion molecule serum fragment is depressed in autism. J Neuropsychiatry Clin Neurosci. 1990;2:413–7.

135. Purcell AE, Rocco MM, Lenhart JA, Hyder K, Zimmerman AW, Pevsner J. Assessment of neural cell adhesion molecule (NCAM) in autistic serum and postmortem brain. J Autism Dev Disord. 2001;31:183–94.

136. Gomez-Fernandez A, de la Torre-Aguilar MJ, Gil-Campos M, Flores-Rojas K, Cruz-Rico MD, Martin-Borreguero P, et al. Children With Autism Spectrum Disorder With Regression Exhibit a Different Profile in Plasma Cytokines and Adhesion Molecules Compared to Children Without Such Regression. Front Pediatr. 2018;6:264.

137. Yang X, Zou M, Pang X, Liang S, Sun C, Wang J, et al. The association between NCAM1 levels and behavioral phenotypes in children with autism spectrum disorder. Behav Brain Res. 2019;359:234–8.

138. Flanagan K, Baradaran-Heravi A, Yin Q, Dao Duc K, Spradling AC, Greenblatt EJ. FMRP-dependent production of large dosage-sensitive proteins is highly conserved. Genetics [Internet]. 2022;221. Available from: http://dx.doi.org/10.1093/genetics/iyac094

139. Xiao W, Adhikari S, Dahal U, Chen Y-S, Hao Y-J, Sun B-F, et al. Nuclear m(6)A Reader YTHDC1 Regulates mRNA Splicing. Mol Cell. 2016;61:507–19.

140. Gokhale NS, Horner SM. RNA modifications go viral [Internet]. PLOS Pathogens. 2017. p. e1006188. Available from: http://dx.doi.org/10.1371/journal.ppat.1006188

141. Edens BM, Vissers C, Su J, Arumugam S, Xu Z, Shi H, et al. FMRP Modulates Neural Differentiation through mA-Dependent mRNA Nuclear Export. Cell Rep. 2019;28:845–54.e5.

142. Kim G-W, Imam H, Siddiqui A. The RNA Binding Proteins YTHDC1 and FMRP Regulate the Nuclear Export of -Methyladenosine-Modified Hepatitis B Virus Transcripts and Affect the Viral Life Cycle. J Virol. 2021;95:e0009721.

143. Jiang X, Liu B, Nie Z, Duan L, Xiong Q, Jin Z, et al. The role of m6A modification in the biological functions and diseases. Signal Transduct Target Ther. 2021;6:74.

144. Zou Z, Wei J, Chen Y, Kang Y, Shi H, Yang F, et al. FMRP phosphorylation modulates neuronal translation through YTHDF1. Mol Cell. 2023;83:4304–17.e8.

145. Lichinchi G, Zhao BS, Wu Y, Lu Z, Qin Y, He C, et al. Dynamics of Human and Viral RNA Methylation during Zika Virus Infection. Cell Host Microbe. 2016;20:666–73.

146. Gokhale NS, McIntyre ABR, Mattocks MD, Holley CL, Lazear HM, Mason CE, et al. Altered m6A Modification of Specific Cellular Transcripts Affects Flaviviridae Infection [Internet]. Molecular Cell. 2020. p. 542–55.e8. Available from: http://dx.doi.org/10.1016/j.molcel.2019.11.007

147. Wang C-X, Cui G-S, Liu X, Xu K, Wang M, Zhang X-X, et al. METTL3-mediated m6A modification is required for cerebellar development. PLoS Biol. 2018;16:e2004880.

148. Bartholomeusz HH, Courchesne E, Karns CM. Relationship between head circumference and brain volume in healthy normal toddlers, children, and adults. Neuropediatrics. 2002;33:239–41.

149. Cheng R-K, Jesuthasan SJ, Penney TB. Zebrafish forebrain and temporal conditioning. Philos Trans R Soc Lond B Biol Sci. 2014;369:20120462.

150. Veenstra-VanderWeele J, O'Reilly KC, Dennis MY, Uribe-Salazar JM, Amaral DG. Translational Neuroscience Approaches to Understanding Autism. Am J Psychiatry. 2023;180:265–76.

151. Rea V, Van Raay TJ. Using Zebrafish to Model Autism Spectrum Disorder: A Comparison of ASD Risk Genes Between Zebrafish and Their Mammalian Counterparts. Front Mol Neurosci. 2020;13:575575.

152. Tayanloo-Beik A, Hamidpour SK, Abedi M, Shojaei H, Tavirani MR, Namazi N, et al. Zebrafish Modeling of Autism Spectrum Disorders, Current Status and Future Prospective. Front Psychiatry. 2022;13:911770.

153. Modeling autism spectrum disorders in zebrafish. Behavioral and Neural Genetics of Zebrafish. Academic Press; 2020. p. 451–80.

154. Sakai C, Ijaz S, Hoffman EJ. Zebrafish Models of Neurodevelopmental Disorders: Past, Present, and Future. Front Mol Neurosci. 2018;11:294.